Review

Research Strategies and Progress in Silicon-Based Anode Materials for Lithium-Ion Batteries

Yuhua Wang , Hongguang Li * , Ying Xu , Yongli Kou , Mingxing Zhao , Wenbo Qi , Ning Zhao

Posted Date: 8 August 2025

doi: 10.20944/preprints202508.0567.v1

Keywords: lithium-ion batteries; silicon negative electrode; silicon-based expansion; anode materials modification and optimization

 doi:10.20944/preprints202508.0567.v1

Review

Research Strategies and Progress in Silicon-Based Anode Materials for Lithium-Ion Batteries

Yuhua Wang [1], Hongguang Li [2,*], Ying Xu [1], Yongli Kou [2], Mingxing Zhao [2], Wenbo Qi [2] and Ning Zhao [3]

[1] Xi'an Peihua University, Xi'an 710125, China
[2] Shaanxi Coal Chemical Industry Technology Research Institute Co., Ltd., Xi'an 710100, China
[3] State Key Laboratory of Coal Conversion, Institute of Coal Chemistry, Chinese Academy of Sciences, Taiyuan 030001, China
* Correspondence: lihg829@126.com; Tel.:+86-029-89282175

Abstract

Lithium-ion batteries (LIBs) have emerged as the predominant power source for portable and mobile energy storage applications, owing to their well-balanced energy density, superior rate capability and excellent cycling stability. However, the relatively low specific capacity of anode materials remains a critical factor limiting further improvement in the energy density of LIBs. Compared with carbon-based anode materials, silicon-based anode materials exhibit significant advantages, including abundant natural reserves and ultrahigh theoretical specific capacity, making them the most promising alternative to graphite anodes. Nevertheless, silicon-based anodes suffer from severe volume expansion during lithiation/de-lithiation processes, as well as structural degradation caused by dynamic cracking of the solid electrolyte interphase (SEI) layer. These issues lead to rapid capacity decay and reduced coulombic efficiency, significantly hindering their industrial application. This review systematically summarizes the failure mechanisms induced by volume expansion in silicon-based anode materials and recent research advancements in multidimensional nanostructure optimization and synergistic composite design strategies. Based on these research advances, a comprehensive comparison is performed among different design and optimization strategies for silicon-based anodes, along with prospective for future performance enhancement. The article provides valuable insights that will facilitate the industrialization of silicon-based anode materials.

Keywords: lithium-ion batteries; silicon negative electrode; silicon-based expansion; anode materials modification and optimization

1. Introduction

Lithium-ion batteries (LIBs) have attracted substantial attention due to their advantageous characteristics, including high operating voltage, low self-discharge rate, stable discharge voltage profile, high energy density, outstanding cycling performance, absence of memory effect, wide operating temperature range and long service life [1]. LIBs are extensively applied in diverse fields such as energy storage, electronic devices, electric vehicles, medical equipment, communications and aerospace [2, 3]. In recent years, with the rapid development of the new energy vehicle and energy storage industries, there is an increasing demand for the energy density of batteries. The energy density of LIBs mainly depends on the electrode materials (cathode and anode) and electrolytes. Selecting anode materials with high specific capacity is an important strategy to achieve the above-mentioned goals. At present, graphite-dominated carbon-based materials serve as the mainstream anode for commercial LIBs. Graphite has the characteristics of abundant reserves, low cost, high electrical conductivity, which favor the intercalation and deintercalation of Li^+ ions as well as low charge-discharge potential. These features make it an ideal anode material for lithium batteries,

 doi:10.20944/preprints202508.0567.v1

accounting for approximately 98% of the market share [4]. Currently, the specific capacity of commercially available graphite materials has reached 360-365 $mAh \cdot g^{-1}$ (theoretical specific capacity, 372 $mAh \cdot g^{-1}$). Consequently, LIBs employing graphite anodes exhibit minimal potential for further energy density enhancement. Compared with graphite, silicon anodes exhibit exceptionally high theoretical specific capacities of 4200 $mAh \cdot g^{-1}$ and 9786 $mAh \cdot cm^{-3}$ [5]. In addition, silicon exhibits a low lithium (de)intercalation voltage plateau (0.2-0.5 V vs. Li^+/Li) during cycling, enabling direct compatibility with commercial cathode materials (e.g., $LiCoO_2$, NCM/NCA) for full-cell configuration [6-8]. The abundant natural reserves and low cost further establish silicon as one of the most promising next-generation anode materials for LIBs [9]. However, due to the alloying reaction for lithium storage, the silicon material undergoes significant volume expansion (up to 300%) during lithiation, leading to the accumulation of internal stress within the material. During charge/discharge cycles, this repeated volume variation causes pulverization of the active material and loss of mechanical integrity in the electrode. It also induces interfacial contact failure between the electrode and electrolyte, along with continuous reconstruction of the solid electrolyte interphase (SEI), resulting in irreversible loss of active Li+ and rapid capacity degradation [10-14]. These issues lead to a decline in the initial coulombic efficiency (ICE) and cycle life of silicon-based LIBs, severely hindering their commercialization. To date, no commercially available silicon-based anode battery has demonstrated exceptionally high performance [9].

This review focuses on the expansion-induced failure mechanisms of silicon-based anode materials. Beginning with an introduction to the working principles of silicon-based LIBs, an in-depth analysis of the expansion mechanisms and associated detrimental effects are provided. Furthermore, recent modification strategies including nanostructured silicon design, silicon-oxygen (SiO_x) composites and silicon-carbon hybrid materials are comprehensively reviewed. Finally, the future development trends and potential applications of silicon-based anodes are discussed.

2. Mechanism of Expansion-Induced Failure in Silicon-Based Anode Materials

The structure of LIBs is generally divided into six components: cathode, anode, SEI, electrolyte, separator and current collector. The cathode typically employs lithium-rich compounds, such as lithium transition metal oxides, including layered metal oxides (e.g., lithium cobalt oxide, lithium nickel oxide, lithium manganese oxide, as well as lithium nickel cobalt manganese oxide and lithium nickel cobalt aluminum oxide) [15, 16], spinel-type oxides (e.g., lithium nickel manganese oxide) [17, 18] and polyanion-type oxides with sulfates, phosphates and silicates (e.g., lithium iron phosphate) [19-21]. Based on the binding mechanism between the anode material and lithium ions, the lithium storage mechanisms of anode materials can be classified into three types: intercalation-type, alloy-type and conversion-type. Silicon-based anodes follow an alloy-type lithium storage mechanism. [22-24]

The cathode and anode are the sites where charge carriers are stored and released during energy storage and delivery in LIBs. Both electrodes enable reversible processes through the intercalation and deintercalation of Li^+ ions. As illustrated in Figure 1, during charging, lithium ions are extracted from the cathode material, migrate through the electrolyte, traverse the separator and subsequently insert the anode material, while electrons flow through the external circuit to the anode. This process transforms the cathode from a lithium-rich phase to a lithium-deficient phase. Conversely, during discharging, lithium ions are extracted from the anode, diffuse through the electrolyte and separator, and re-insert the lithium-deficient cathode, with electrons returning via external circuit. Throughout the charge-discharge cycles, lithium ions shuttle between the cathode and anode, leading to the colloquial term “rocking-chair battery” for LIBs. [25, 26]

 doi:10.20944/preprints202508.0567.v1

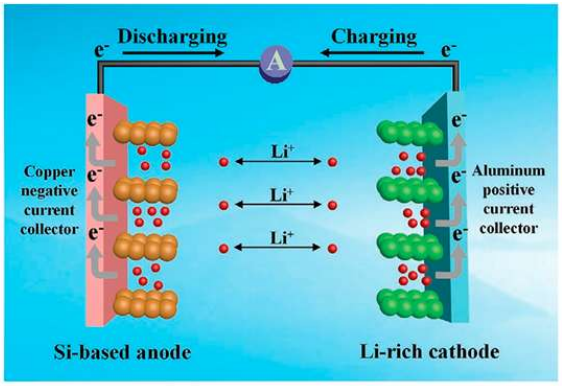

Figure 1. Schematic illustration of the reaction of the LIB. [22].

During the initial lithiation, crystalline silicon undergoes phase transition from crystalline to amorphous state and remains the amorphous phase thereafter. The lithium (de)intercalation process in silicon-based anodes corresponds to the de-lithiation of lithium-silicon alloys and the formation of lithium-silicon alloy phases (Li_xSi). Under ideal high temperature lithiation conditions, the alloying reaction between Li and Si involves multiple phase transformations (as illustrated in Figure 2), sequentially forming four distinct alloy phases: $Li_{12}Si_7$, Li_7Si_3, $Li_{13}Si_4$, and $Li_{22}Si_5$. The theoretical specific capacity reaches a remarkable 4200 mAh·g^{-1} upon the formation of $Li_{22}Si_5$. At room temperature, different lithium-silicon compounds form at various lithiation stages. When $Li_{15}Si_4$ is formed, the theoretical specific capacity remains as high as 3580 mAh·g^{-1}, nearly 10 times that of graphite anode materials, demonstrating exceptional lithium storage capability.[27-31] The first discharge (lithiation) curve of silicon exhibits a long, low-voltage plateau, corresponding to the phase transition from crystalline silicon to amorphous lithium-silicon alloy [29]. When the discharge potential drops below 0.05 V, the crystalline $Li_{15}Si_4$ phase emerges [32], which subsequently partially transforms back into amorphous state during the charging process.

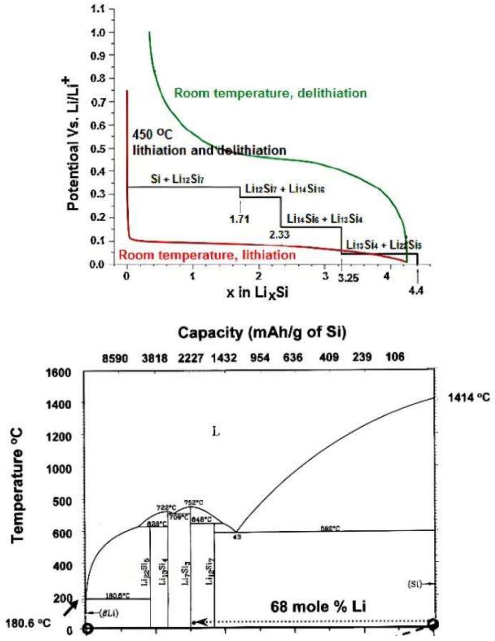

Figure 2. Lithium storage mechanisms and phase-capacity diagrams of Si-based anode materials: (a) Lithiation mechanism of Si at room temperature and high temperature [29]; (b) Phase diagram and capacity correspondence diagram of Li-Si alloy [33].

 doi:10.20944/preprints202508.0567.v1

The first lithiation plateau of silicon appears at 0.1 V (vs. Li^+/Li), corresponding to the transformation of crystalline silicon (c-Si) into amorphous Li_xSi (a-Li_xSi), during which c-Si and a-Li_xSi coexist as distinct phases. This persists until the voltage drops below 50 mV, where a-Li_xSi further crystallizes into $Li_{15}Si_4$ phase (c-$Li_{3.75}Si$). The complete phase transformation mechanism proceeds as follows [34-36]:

The initial lithiation process:

$$c\text{-}Si + x\ Li^+ + x\ e^- \rightarrow a\text{-}Li_xSi$$

$$a\text{-}Li_xSi + (3.75\text{-}x)\ Li^+ + (3.75\text{-}x)\ e^- \rightarrow c\text{-}Li_{3.75}Si$$

The initial de-lithiation process:

$$c\text{-}Li_{3.75}Si \rightarrow a\text{-}Li_xSi + (3.75\text{-}x)\ Li^+ + (3.75\text{-}x)\ e^-$$

$$a\text{-}Li_xSi \rightarrow a\text{-}Si + x\ Li^+ + x\ e^-$$

Subsequent lithiation cycles:

$$a\text{-}Si + x\ Li^+ + x\ e^- \rightarrow a\text{-}Li_xSi$$

$$a\text{-}Li_xSi + (3.75\text{-}x)\ Li^+ + (3.75\text{-}x)\ e^- \rightarrow c\text{-}Li_{3.75}Si$$

De-lithiation Process:

$$c\text{-}Li_{3.75}Si \rightarrow a\text{-}Li_xSi + (3.75\text{-}x)\ Li^+ + (3.75\text{-}x)\ e^-$$

$$a\text{-}Li_xSi \rightarrow a\text{-}Si + x\ Li^+ + x\ e^-$$

During the charge-discharge process, silicon combines with lithium ions to form Li-Si alloys, accompanied by the flow of electrons. Silicon-based anode materials possess a larger space for lithium ion intercalation compared to lithium metals. During the discharge process, lithium ions intercalate into the silicon lattice which can accommodate more lithium ions, thereby enhancing the specific capacity of the battery. Observations via X-ray diffraction (XRD) and high-resolution transmission electron microscopy (HRTEM) have revealed the limited lithiation of crystalline silicon: crystalline phases are first formed, followed by an amorphous phase transition, resulting in lithiated amorphous silicides. [37]

Moreover, Liu et al. [38] observed, using in situ transmission electron microscopy (TEM), a sharp interface (approximately 3-4 atomic layers thick) between crystalline silicon and amorphous lithium-silicon alloys. The study indicated that the crystalline-to-amorphous phase transition occurs through the layer-by-layer peeling of atomic planes, leading to the orientation-dependent mobility of the interface. At the atomic scale, Liu et al. proposed that silicon crystals at the interface break into isolated silicon atoms or silicon atom pairs, which are encapsulated in the lithium-rich amorphous phase. The sharp interface physically manifests the high activation energy required for breaking Si-Si bonds. This phenomenon is consistent with the findings by Key's research group via in situ nuclear magnetic resonance (NMR), which revealed that the first lithiation occurs through the formation of isolated silicon atoms and Si-Si clusters embedded in the lithium matrix [39]. Researchers also observed the anisotropy in the lithiation of silicon i.e., silicon exhibits different expansion tendencies along various axes. Through the analysis of reaction peaks, it is demonstrated that the anisotropic lithiation and expansion primarily result from the differences in interfacial mobility among different crystal planes [40], which provides a theoretical basis for silicon expansion from a crystallographic perspective.

During the lithiation process, the Si-Si bonds in crystalline silicon are broken, resulting in the formation of an amorphous product, a-Li_xSi ($0 < x < 3.75$) [41]. Ding et al. found that there are at least two phase transition processes corresponding to the formation of a-$Li_{2.1}Si$ and a-$Li_{3.3}Si$, respectively [42]. Bordes found that a core-shell structure coated with $Li_{3.1}Si$ is formed after lithiation of silicon [43]. During the lithiation process, lithium diffuses inward through the crystal planes between different grains, leading to gradient structure where the exterior is lithium-rich and the interior is lithium-poor. With further lithiation, it was found through X-ray powder diffraction technology that the amorphous Li_xSi transforms back into the crystalline $Li_{15}Si_4$ ($Li_{3.75}Si$, corresponding to a capacity of 3579 $mAh \cdot g^{-1}$) at a potential of 50 mV vs. Li/Li^+ [32], This crystallization process has also been confirmed by in-situ TEM [44-47]. According to theoretical calculations, the crystallization of Li_xSi to form $Li_{3.75}Si$ has been proven to be a spontaneous process, which is only related to the concentration

 doi:10.20944/preprints202508.0567.v1

of intercalated lithium instead of long-range diffusion [44]. The $Li_{15}Si_4$ phase is highly reactive, leading to side reactions that are detrimental to the long-term cycling performance of the electrode [39]. The formation of $Li_{15}Si_4$ is considered to accelerate the degradation of silicon electrodes. It has been demonstrated that better cycling stability can be achieved only when the electrode is cycled above 50 mV [32, 48, 49]. During the de-lithiation process, the crystalline $Li_{15}Si_4$ phase firstly transforms into amorphous Li_xSi through a two-phase reaction (at 50 mV) [32]. Subsequently, de-lithiation is completed via amorphous-to-amorphous phase transition [50]. Most studies have shown that only a single phase transition occurs during the de-lithiation of amorphous Li_xSi ($0 < x < 3.75$) [32, 50, 51].

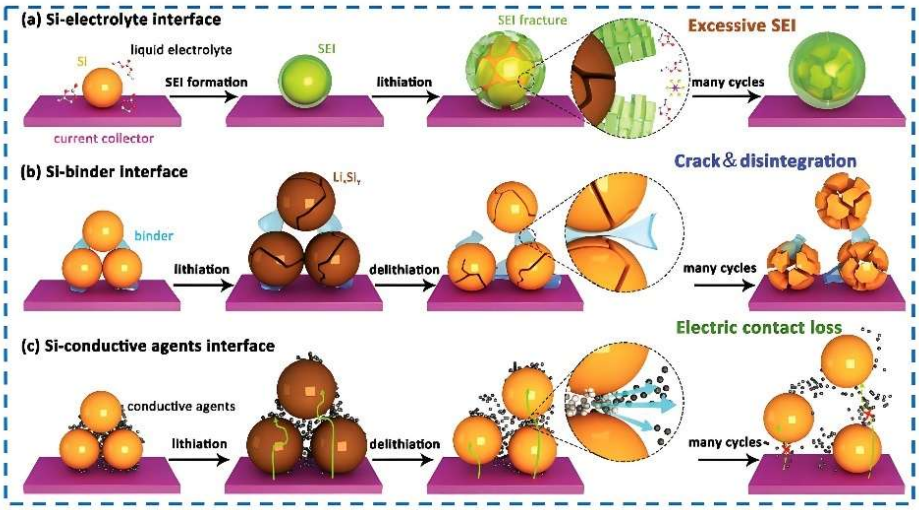

Figure 3. Schematic of the evolution process of failure mechanisms in silicon-based anode materials [31].

The theoretical specific capacity of silicon calculated based on the $Li_{22}Si_5$ phase is 4200 $mAh \cdot g^{-1}$, with a net volume increase of 310% during the lithiation and de-lithiation processes [52]. Liu et al. investigated the lithiation of individual silicon nanoparticles using real-time in-situ transmission electron microscopy (TEM) and found that the diameter of a single 80 nm spherical silicon nanoparticle increased to 130 nm after complete lithiation, corresponding to a net volume expansion of approximately 300% [53]. The evolution of the failure mechanism of silicon-based anode materials is shown in Figure 3. Such repeated volume expansion and contraction during lithiation and de-lithiation lead to electrode pulverization, thereby losing electrical contact between the active material-current collector interface, which is exactly the reason for the generally rapid capacity fading of silicon-based anode batteries [34].

SEI film is formed by the reaction between electrode and electrolytes at the solid-liquid interface during the first charge-discharge cycle of the battery. The SEI film allows rapid transport of lithium ions while blocking the passage of electrons. Although the formation of the SEI film consumes lithium ions, it can prevent direct contact between the electrolyte and active materials, thereby reducing the occurrence of side reactions. A stable SEI film is a prerequisite for the stable operation of the electrode [54]. However, the volume change of Si in silicon-based anode will damage the SEI film and expose new electrode surfaces, leading to continuous formation of the SEI film on the surfaces of fragmented silicon material pieces. Such a process will render the SEI film on the surface of the silicon anode unstable [55, 56]. Moreover, the continuous growth of the SEI film constantly consumes lithium sources, which will reduce the coulombic efficiency and capacity of the battery [38]. In addition, the thickened SEI film will also increase the internal resistance of the battery, resulting in increased electrode polarization and reduced capacity. [57, 58]

Moreover, the electronic conductivity of Si is 10^{-5}-10^{-3} $S \cdot cm^{-1}$, and the Li^+ diffusion rate is 10^{-14}-10^{-12} $cm^2 \cdot s^{-1}$, which restrict the reaction kinetics during the lithiation process. Consequently, the

 doi:10.20944/preprints202508.0567.v1

advantage of the high capacity of active Si cannot be fully exploited, severely hindering the practical application of Si-based anodes. [59, 60]

In summary, despite the advantages of silicon-based anodes such as high specific capacity, low lithium intercalation potential and abundant resources, the challenges posed by volume changes caused by alloying reactions during the lithiation and de-lithiation processes have severe impacts on battery performance. Therefore, it is urgent to address the series of issues to promote the advancement of battery technology.

3. Modification Design and Optimization of Silicon-Based Anode Materials

To address the problems and challenges caused by volume expansion of silicon-based anodes during battery reactions, researchers have adopted the methods such as nanonization, thin-film formation, porous structure construction and composite preparation of silicon-based materials to buffer or reduce the alternating stress during lithiation and de-lithiation processes, thereby mitigating the volume effect, improving the structural stability of the material and inhibiting the excessive growth of the SEI film [61-64]. The following content will focus on multi-dimensional nanostructured silicon design, preparation and structural optimization of SiC composite materials as well as pre-lithiation and modification of SiO_x. Based on the latest design strategies and achievements in silicon-based anode materials, it is expected to provide some valuable insights for silicon-based anode materials.

3.1. Multi-Dimensional Nanostructured Silicon Materials

Nanostructure design is one of the most effective methods to accommodate the volume changes through which silicon anodes can relieve the alternating mechanical stress by virtue of the structural advantages in the surrounding free space. Moreover, nanostructured silicon, due to its higher specific surface area and larger binding energy between atoms, can effectively release the pressure during volume expansion of silicon particles, preventing the material from collapsing after undergoing expansion and contraction, thereby maintaining its cycling stability. Currently, silicon-based nanomaterials can be classified by dimension into zero-dimensional (such as silicon nanoparticles, porous silicon, hollow silicon, etc. [65, 66]), one-dimensional (such as silicon nanowires, silicon nanotubes, etc. [67-71]) and two-dimensional nanomaterials (such as silicon nanofilms [72]).

Liu et al. determined a critical diameter of 150 nm: particles with diameter below the critical value do not crack during the first lithiation, while those with diameter exceeding this value firstly develop surface cracks, which lead to overall fracture during further expansion [53]. Other results indicated that nanostructures reserve a certain space for the expansion, increase the threshold for material pulverization [73, 74], and thus improve the cycling performance of silicon-based anodes to a certain extent. Reducing the size of silicon materials to nanoscale significantly shorten the diffusion path of lithium ions, thereby increasing the diffusion rate of lithium ions and the insertion/extraction rate. In addition, nanostructures can effectively suppress the stress generated by the volume change of silicon during charge-discharge processes, thereby improving the cycling stability of the material. Considering that smaller-scale particles have higher specific surface area and porosity, which can effectively relieve the stress and strain caused by volume expansion, researchers have carried out extensive work on the design of silicon-based materials over the past decade. At present, some applicable nanomaterials have been prepared using the nano-crystallization of silicon materials, including nanotubes [75], nanowires [76], nanocomposites [77], nanofilms [78, 79] and nanoporous structures [80].

3.1.1. Zero-Dimensional Nanostructured Silicon Materials

Yao et al. prepared a kind of hollow silicon via chemical vapor deposition, which exhibits excellent cycling performance [65]. Ge et al. reported a porous silicon material synthesized by doping-etching method [66]. Commercial silicon nanoparticles were firstly doped with boron (B) and then

 doi:10.20944/preprints202508.0567.v1

were etched using a mixed solution of $AgNO_3$ and HF, resulting in porous silicon with specific surface area exceeding 60 $m^2 \cdot g^{-1}$. Benefiting from B doping, the porous silicon contains numerous mesopores, which endow the sample with good cycling performance.

Currently, porous silicon is mainly prepared by template methods [81]. Li et al. fabricated porous silicon using electrochemically etching and boron-doped silicon wafers to investigate the relationship between the porous structure and silicon-lithium alloying [82]. Ge et al. prepared fine and uniform powders from large silicon spheres by ball milling. Then metal elements such as iron and aluminum were removed through chemical etching to obtain nanoscale porous silicon materials. The as-prepared porous silicon anode material have stable reversible specific capacity which retain specific capacity of 1100 $mAh \cdot g^{-1}$ after 600 cycles at current density of 2 $A \cdot g^{-1}$ [83].

Yu et al. reported that porous silicon was formed by magnesiothermic reduction of mesoporous silica [84] that contains large number of pores with diameters larger than 50 nm, around which crystalline silicon with diameter of 10 nm is distributed. The overall expansion rate of the material is related to the pores and the skeleton size of the structure. The presence of pores reduces the overall volume change rate of the porous silicon to 30%. Hwang et al. also prepared porous silicon materials via magnesiothermic reduction, which showed stable charge-discharge cycling performance [85]. Magnesiothermic reduction is a scalable and efficient technology that can produce high-quality silicon at a lower temperature and in a shorter time. Future research can focus on increasing silicon content, improving long-term performance and optimizing the interface between the anode and electrolyte, among other aspects.

Despite the certain achievements made in the aforementioned studies, nano-silicon tends to agglomerate due to the nanoscale size effect in practical applications. Once nano-silicon particles agglomerate, the superposition of their mutual volume changes will lead to uneven stress in the electrode sheet on a macroscopic scale, resulting in the destruction of the electrode sheet and poor cycling performance.

3.1.2. One-Dimensional Silicon Nanostructures

Silicon nanowires exhibit significant advantages [86] of micrometer-scale space in the longitudinal direction, which allows the growth of layered structures and increases the effective surface area for electrochemical reactions; the micrometer-scale size in the longitudinal direction can form a dense and entangled network, providing structural rigidity and better adhesion compared to silicon nanoparticles; silicon nanowires can be directly grown on current collectors to eliminate the need for conductive agents and binders, thereby enhancing the energy density; the high aspect ratio of silicon nanowires effectively increases the electrode-electrolyte contact area, promoting the full utilization of the capacity of silicon materials; the nanoscale size of silicon nanowires in the transverse direction shortens the lithium ion transport path, facilitating high-rate charge-discharge processes. Moreover, the gaps between nanowires/nanotubes can well buffer the stress caused by the volume effect, further improving the cycling performance [86-88].

Cui et al. [68] successfully prepared silicon nanowires on a stainless steel substrate using gold as catalyst as early as 2008. The results showed that silicon nanowires can withstand large strains without pulverization, provide good electronic contact and conduction as well as strong lithium insertion/extraction performance. They also founded an enterprise specializing in the production of silicon nanowires, promoting the commercial application of pure silicon anodes. However, due to the high manufacturing cost, they are currently mostly used in some high-end demonstration projects and have not yet been applied on a large scale.

In addition, Park et al. reduced and decomposed silicon precursors in an alumina template followed by etching to prepare silicon nanotubes with extremely high reversible capacity of 3247 $mAh \cdot g^{-1}$ [89]. After 200 cycles, the capacity was still nearly 10 times higher than that of graphite.

Other studies showed that surface modification of silicon nanowires or fabrication into nanotubes can enhance the electrochemical performance. However, while the abundant surface area enables deep lithium insertion and rapid extraction, it also leads to more intense side reactions

 doi:10.20944/preprints202508.0567.v1

between the surface and the electrolyte, resulting in low ICE, which limits their commercial application [90-92].

3.1.3. Two-Dimensional Nanostructures

Silicon nanofilms deposited on the surface of electrode materials can adapt to the stress generated by volume expansion and contraction while maintaining the mechanical integrity [93, 94]. Li et al. proposed that the volume expansion during lithiation occurs perpendicular to the film surface. However, during de-lithiation, volume contraction takes place both in the planar and vertical directions of the film [95]. Yu et al. adopted a new stress-relief strategy for films using polydimethylsiloxane as an elastic substrate. The volume strain of silicon during electrochemical cycling can be regulated by the elastic substrate. The electrode keeps capacity of 3498 $mAh \cdot g^{-1}$ with capacity retention rate of 84.6% after 500 cycles at current density of 0.25 C [96]. Elomari et al. prepared silicon nanofilms with different thicknesses via direct current (DC) magnetron sputtering deposition with low density and large grain size. The discharge capacities of the electrodes with thicknesses of 600 nm and 1000 nm are 800 $mAh \cdot g^{-1}$ and 406 $mAh \cdot g^{-1}$, respectively. In addition, these electrodes exhibit excellent ICE, among which the 1000 nm-thick electrode achieves an ICE of 96.08% [97]. Although two-dimensional silicon nanofilms, as anode materials, have advantages of suitable working potential, abundant reserves and improved ICE, they still face the challenges of rapid capacity fading and shortened cycle life. Future breakthroughs need to integrate micro-nano structure design, interface optimization and process innovation to realize the commercial application.

3.1.4. Secondary Structural Design of Silicon Nanomaterials

Compared with silicon-based nanoparticles, secondary particles possess two major advantages: higher coulombic efficiency and higher areal specific capacity. By adjusting the size of silicon-based secondary particles, the contact area between silicon-based nanomaterials and the electrolyte can be appropriately reduced, which helps to decrease excessive consumption of the electrolyte and improve the coulombic efficiency.

Liu et al. prepared a silicon-based anode with pomegranate-like structure. Silicon particles with yolk-shell structure (with a particle size of approximately 80 nm) were integrated into cluster structures with sizes ranging from 1 to 10 μm. Subsequently, graphene layer was coated to prevent direct contact between the silicon material and the electrolyte. In addition to stabilizing the interface, the graphene shell can enhance the electrical conductivity of the entire structure, which is beneficial for improving the ICE [98]. Li et al. introduced conductive graphene cages as an encapsulation layer to stabilize the silicon particle electrodes in batteries. The graphene cages, with mechanical strength and flexibility, have pre-designed void spaces that can confine all fragmented silicon pieces inside. Meanwhile, the graphene cages can act as an electrolyte barrier, enabling the SEI film to form mainly on the outer surface of the graphene cages. This structure can effectively reduce the consumption of active materials caused by irreversible processes and improve the ICE [99]. Wang et al. synthesized silicon nanoparticles into clusters using a bottom-up microemulsion method. Then, a dense silicon shell was coated via CVD. Finally, a graphene cage was wrapped. After coating the silicon shell, the formation of SEI on the outer surface can be restricted, making the structure highly pressure-resistant. The encapsulation with graphene cages improves the coulombic efficiency. The material exhibits high specific capacity of up to 2041 $mAh \cdot cm^{-3}$, coulombic efficiency of >99.5% and good stability even in the fully charged state [100].

Although a considerable number of silicon nanostructures have been reported as anode for LIBs, all nanostructured silicon materials exhibit a certain degree of capacity fading, which greatly hinders their practical application.

3.2. SiC Anode Materials

 doi:10.20944/preprints202508.0567.v1

Although the volume expansion of silicon-based anodes has been effectively alleviated through nanostructure design, and their cycling stability has been significantly improved, the issue of sluggish charge transport kinetics remains prominent due to the intrinsic properties of semiconductor materials. This conductivity defect not only exacerbates electrode polarization but also severely restricts the achievement of high-rate performance [101]. To address the low conductivity of silicon, researchers have attempted to construct composite structures to enhance the electrical conductivity of silicon-based anodes. Among them, carbon has attracted much attention due to its excellent electrical conductivity, good shrinkage property and low cost. In addition, carbon materials can stabilize the structure of silicon anodes and effectively suppress the volume stress of silicon materials during lithiation and de-lithiation processes to improve cycling performance. Therefore, silicon-carbon composites have become an effective strategy to address the challenges of silicon-based anodes [99, 102-107].

Currently, the methods for preparing silicon-carbon composite anode materials include chemical vapor deposition (CVD) [108], spray drying [109], magnesiothermic reduction [110], mechanical ball milling [111], sol-gel method [112] etc. Despite the differences in preparation methods, the core idea is to nanocrystallize silicon and the combination with carbon to construct corresponding composite structures.

3.2.1. Mechanical Mixing Method

The simplest approach to prepare silicon-carbon composite anodes is mechanically mix carbon materials with nano-silicon. Due to the size difference, nano-silicon can fill the gaps between graphite particles, and the pores can be utilized to buffer volume changes. Meanwhile, the carbon material matrix can mechanically buffer the volume variations [113, 114]. Wang et al. prepared silicon-carbon anode materials by mechanically mixing nano-silicon particles with graphite using ball milling [114]. The initial specific capacity can reach 1039 $mAh \cdot g^{-1}$. However, only 794 $mAh \cdot g^{-1}$ is retained after 20 cycles. This is because nano-silicon tends to agglomerate and there is no interaction between nano-silicon and graphite. During the lithiation and de-lithiation processes, the significant difference in volume change between nano-silicon materials and carbon materials still leads to rapid loss of electrical contact, resulting in capacity fading [115-117].

3.2.2. Binder Design

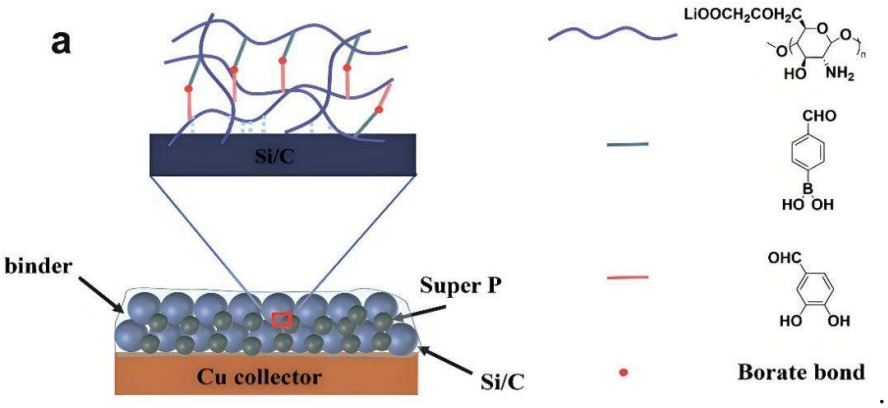

 doi:10.20944/preprints202508.0567.v1

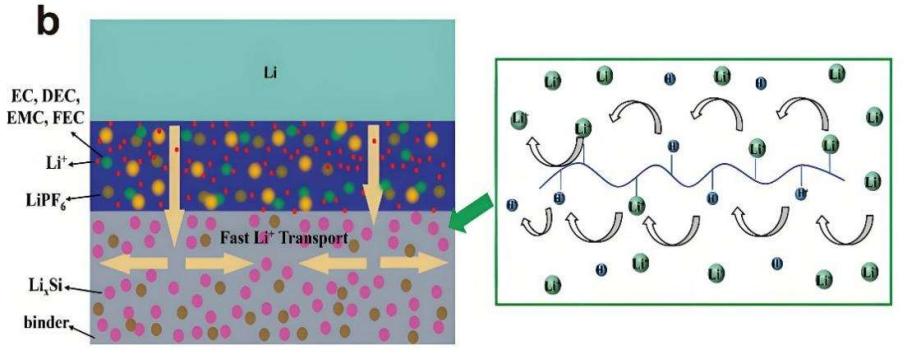

Figure 4. a) Schematic illustration of the mechanism of cross-linking for LiCB complexes and their interaction. b) Schematic diagram of the lithium ion transfer process.[117].

Adopting appropriate binder is also an effective strategy to address the volume expansion of silicon-based anode materials. An ideal binder should possess good adhesiveness to uniformly coat on the electrode sheet, enhance the overall stability of the electrode without hindering ion transport, reduce the shedding of active materials as well as improve the electrochemical performance and lifespan of the battery.

Li et al. prepared a self-healing binder with robust mechanical properties through pre-lithiation of carboxymethyl chitosan and dynamic cross-linking of borate ester (Figure 4) [117]. Benefiting from the excellent adhesion properties of this pre-lithiated chitosan network binder (LiCB), the ICE of the nano-silicon/graphite composite anode reached 82.18%, 7.3% higher than that of the nano-silicon/graphite composite anode using only PAA binder. Moreover, the O sites of the -COOH groups in the structure can act as hopping nodes in promoting lithium ion transport and enhancing the charge transfer between lithium ions and the electrode surface. As a result, the high-rate discharge performance is superior to that of the nano-silicon/graphite composite anode using only polyacrylic acid (PAA) binder. In addition, the borate ester bonds form a cross-linked network, ensuring strong binding affinity with nano-silicon in the carbon gel phase, maintaining the structural integrity of the nano-silicon/graphite composite anode during cyclic charge-discharge processes, and improving cycling stability.

Substances rich in hydroxyl and carboxyl groups [113, 115, 116, 118] can also enhance the ability of nano-silicon-carbon anodes to resist volume stress due to their strong binding force with nano-silicon. In particular, grafting the functional groups onto three-dimensional conductive networks such as carbon nanotubes to achieve strong contact between silicon particles and the three-dimensional framework can further improve the rate performance and cycling stability of silicon-based anodes [113].

Wang et al. developed an aqueous binder (PVA-g-M) based on polyvinyl alcohol (PVA) grafted with methacrylic acid (MAA) for Si/C anodes [119]. The introduction of carboxyl groups from MAA enables PVA-g-M to form more hydrogen bonds, enhancing the cohesion of the binder film and its adhesion to the silicon-based surface. In addition, the methyl-containing segments of MAA can wet the carbon-based surface, thereby strengthening the adhesion between PVA-g-M and carbonaceous materials. The Si/C anode prepared with the PVA-g-M binder can significantly inhibit the electrode volume expansion during cycling, maintain high structural integrity, form an SEI with a high lithium fluoride content which exhibits excellent cycling stability (with capacity retention rate of 81.1% after 300 cycles).

Yan et al. adopted a dual-conductive high-strength and tough binder to alleviate volume expansion, inhibit repeated formation of SEI and improve the electrochemical reaction kinetics of μSi electrodes [120]. A new type of binder (marked as PPG) was successfully prepared through thermal cross-linking of "hard" polyacrylic acid (PAA) and “soft” polyvinyl alcohol (PVA), combined with conductive graphene. The as-prepared μSi electrode (μSi-PPG) exhibited excellent electrochemical

 doi:10.20944/preprints202508.0567.v1

reaction kinetics, highly intact electrode structure, as well as dense and stable SEI during electrochemical cycling. The μSi-PPG electrode showed outstanding electrochemical performance, retaining the high capacity of 1913.1 $mAh \cdot g^{-1}$ after 1000 cycles at 1C with capacity retention rate of 86.7%. More importantly, the electrode still maintains an ultra-high capacity of 1451 $mAh \cdot g^{-1}$ at a high rate of 5C.

In addition, Zhang et al. synthesized a functional polymer PIL-AA with cyano and carboxyl groups through free radical polymerization of ionic liquid monomer (IL-CN) and acrylic acid. By mixing PIL-AA with polyvinyl alcohol (PVA) solution, a cross-linkable binder can be obtained [121]. The cyano groups on PIL-AA can react with the hydroxyl groups on PVA chains via Ritter reaction, enabling the binder to achieve in-situ cross-linking through amide groups, thus preparing the c-PIAV binder. This binder is capable of inhibiting the pulverization of silicon (Si) particles and alleviating the volume change of silicon-carbon (Si-C) anodes. The c-PIAV@Si-C||Li coin cell shows good long-term cycle performance and C-rate performance.

In summary, the design of binders for silicon-based anodes needs to comprehensively consider the material's elasticity, adhesive force, conductivity, electrochemical stability and environmental friendliness. Through reasonable binder selection and structural design, the challenges faced by silicon anodes can be overcome to a certain extent, and the performance and lifespan of LIBs can be improved.

3.2.3. Chemical Vapor Deposition Method

A simple and efficient preparation approach involves depositing silicon on carbon matrix materials via chemical vapor deposition (CVD) technology, followed by carbon coating. The selection of carbon matrix materials plays a decisive role: carbon matrices with different microstructures and physicochemical properties significantly affect the deposition behavior of silicon and the interfacial bonding characteristics between silicon and the carbon matrix, thereby leading to significant differences in the electrochemical performance of the final composites. A suitable pore volume, large specific surface area and abundant micropores are more favorable for carbon matrix precursors.

Yi et al. prepared phosphorus-doped porous hard carbon as a substrate for silicon deposition (Figure 5) [122]. Compared with graphite substrates, the pore formed by phosphorus-doped porous hard carbon can accommodate the volume expansion of silicon. Additionally, the higher graphitization degree is beneficial for lithium intercalation, thereby improving the coulombic efficiency. The as-prepared material exhibits an initial charge capacity of 1124 $mAh \cdot g^{-1}$ at current density of 0.1C, with an ICE of 83.2%.

Liu et al. deposited silicon on a composite carbon matrix composed of carbon nanotubes and graphene [123]. Firstly, a three-dimensional conductive structure consisting of carbon nanotubes and graphene was constructed using spray-drying. Subsequently, silicon was grown on the carbon skeleton via silane CVD to obtain the composite material GC-Si. Finally, a mixed gas of CH_4 and Ar was introduced into the PECVD reactor to grow a carbon layer, forming the GC@Si-C composite. This composite demonstrates high initial specific capacity of 2050 $mAh \cdot g^{-1}$ and an ICE of 80%. Moreover, it maintains capacity retention rate of 98.7% after 150 cycles at current density of 0.5 $A \cdot g^{-1}$, with excellent rate performance.

 doi:10.20944/preprints202508.0567.v1

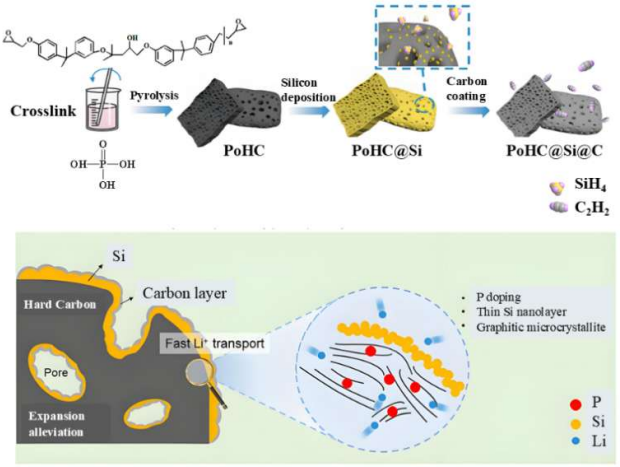

Figure 5. Schematic of preparation process and material for PoHC@Si@C [122].

In addition, using metal-organic framework materials (ZIFs) as carbon matrix precursors can yield porous carbon materials with uniform and controllable size, morphology and micropore diameter. The as-synthesized silicon-carbon material exhibits a volume expansion rate of only 20% after cycling even at an extremely high silicon content (60%), which effectively restricts the volume expansion of silicon [124].

Through precise regulation of process parameters, chemical vapor deposition (CVD) can achieve accurate control over coating thickness, uniformity and particle size distribution of the thin film. The prepared silicon-carbon anode materials have realized significant improvements in key performance indicators such as initial charge-discharge efficiency, cycling stability and volume expansion rate. However, to realize large-scale application of this technology, technical bottlenecks in aspects like batch stability, cost control and safe production still need to be addressed.

3.2.4. Structural Design Optimization

To further enhance the electrochemical performance of silicon-carbon anode materials, researchers have constructed three-dimensional frameworks using carbon materials to buffer the significant volume expansion of silicon during lithiation/de-lithiation processes and improve the overall electrical conductivity.

Li et al. successfully prepared carbon-coated core-shell structured nano-silicon@carbon through the following process: nano-silicon particles were obtained by ball-milling sawdust from the photovoltaic industry. Then, metal impurities were removed by hydrochloric acid while organic impurities were eliminated via heat treatment [125]. The purified nano-silicon was wet-mixed with phenolic resin to form a precursor, and finally, the phenolic-resin was pyrolyzed at high temperature to achieve carbon coating. The core-shell structure enhances the electrical conductivity of the silicon-carbon anode, promotes the movement of ions/electrons and reduces the volume fluctuation of silicon during lithiation/de-lithiation processes. Compared with pure silicon anodes, the Li^+ transport efficiency of nano-Si@C is significantly improved, exhibiting better cycling and rate performance. At current density of 0.5 $A \cdot g^{-1}$, the specific capacity of nano-Si@C is 440 $mAh \cdot g^{-1}$ higher than that of pure silicon anodes after 150 cycles, demonstrating more excellent cycling performance.

Xu et al. prepared a watermelon-like structured silicon-carbon anode material through multi-step process: firstly, a suspension was formed by mixing nano-silicon particles with polyvinylpyrrolidone and glucose using CMC as a dispersant, followed by the addition of flake graphite. After dispersion via ball milling, the mixture was spray-granulated into microspherical particles, which were then pyrolyzed and carbonized at 900 °C. Finally, a carbon layer was coated via acetylene-based vapor phase carbon deposition [126]. In this structure, the nano-silicon cores contribute to a specific capacity of 620 $mAh \cdot g^{-1}$ for the anode. The carbon framework and coating

 doi:10.20944/preprints202508.0567.v1

layers from the interior to the exterior effectively prevent electrolyte erosion. Moreover, the nano-sized silicon particles are uniformly assembled into silicon-carbon microspheres rather than agglomerates, further reducing the probability of electrolyte side reactions, thus achieving an initial charge-discharge coulombic efficiency of 89.2%. Benefiting from the dual protection strategies of the layered buffer structure and optimized size distribution, the watermelon-like structured silicon-carbon microspheres exhibit excellent cycling stability with capacity retention rate exceeding 80% after more than 500 cycles, as well as high rate performance with 80% capacity retention at 5C.

The watermelon-like structured silicon-carbon materials with excellent electrochemical performance [127, 128] prompted researchers to further construct pomegranate-type silicon-carbon materials (Figure 6) [129, 130] through the hydrolysis of organic carbon sources coupled with carbonization. The resulting nano-silicon particles, after being coated with carbon layer, are embedded in mesoporous "pomegranate carbon chambers" like "pomegranate seeds", with 3.4 nm pores filled between them [131]. The porous carbon network framework not only ensures good electrical conductivity but also adapts to the significant volume changes during cycling, promoting the rapid diffusion of lithium ions. Furthermore, substances such as silicon oxides can be added between the silicon core and the carbon layer, and the covalent bonds between carbon, silicon and oxygen can enhance the binding force between the silicon core and the carbon layer, thereby improving the cycling performance of the material [131]. When paired with $LiCoO_2$ to form a full cell, it can maintain a capacity retention rate of 87.9% after 300 cycles. To enhance its electrical conductivity, graphene materials have also been incorporated to construct layered pomegranate-type silicon-carbon anode [129]. The outer graphene, acting as an inner membrane and outer shell, can accelerate ion and electron transport rates and further buffer the volume change of the internal silicon, thus effectively improving the cycling stability and rate performance of the silicon-carbon material.

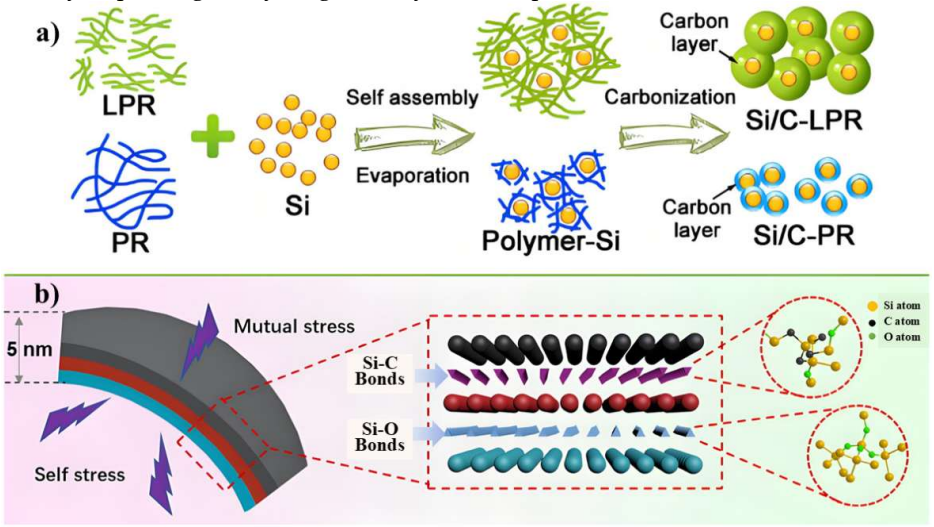

Figure 6. a) Flow chart for the preparation of Si/C-LPR nanocomposites [130]. b) Hierarchical structure of the HPS-Si anode [131].

The watermelon-like and pomegranate-like silicon-carbon composites formed by the aggregation of core-shell structures are limited by the size of nano-silicon particles. When the size of nano-silicon particles is relatively large, the protective shell on the surface may crack during long-term cycling, simultaneously transmitting this stress to the entire micron-scale particle. Eventually, the overall particle disintegrates, leading to the destruction of the electrode structure. Therefore, yolk-shell structured silicon-carbon composites have been developed (Figure 7) [132]. In this structure, multiple small-sized silicon nanoparticles are encapsulated within a double-layered porous carbon shell. This double carbon layer effectively prevents electrolyte penetration, increasing the ICE to 71%, which rapidly rises to 90% in the second cycle. The internal voids within the structure accommodate the volume expansion of silicon particles during lithiation, reducing stress on the outer carbon layer.

 doi:10.20944/preprints202508.0567.v1

Under the dual buffering effect of the carbon layer and voids, this material exhibits an initial specific capacity as high as 2108 mAh·g^{-1} and maintains stable capacity retention over 200 cycles.

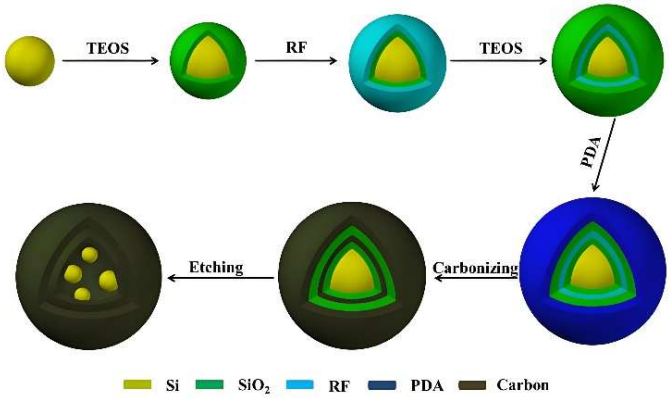

Figure 7. Schematic illustration of the preparation process of yolk-shell structured Si/C composites [132].

In addition, silicon-carbon materials with hollow structures have been prepared to cope with the severe volume expansion of silicon during lithiation [133-135]. Li et al. coated an alumina layer and then a carbon layer on the surface of silica particles [133]. After removing the alumina layer, the inner silica was reduced to silicon via magnesiothermic reduction. Finally, the hollow-structured silicon-carbon anode material was obtained after removing magnesium oxide and residual magnesium metal with hydrochloric acid (Figure 8). The porous design of the silicon core not only inhibits the volume expansion but also forms some pores to buffer the expansion of silicon, thus improving the cycling performance of the silicon anode. Such hollow-structured composites can also be prepared by reducing silicon oxide and etching zinc oxide nanorod templates to in-situ synthesize hollow silicon nanotubes (Figure 8) [135]. The prepared HSiNTs/CC anode displays superior performance with large reversible capacity, high cyclic stability performance and good rate capability.

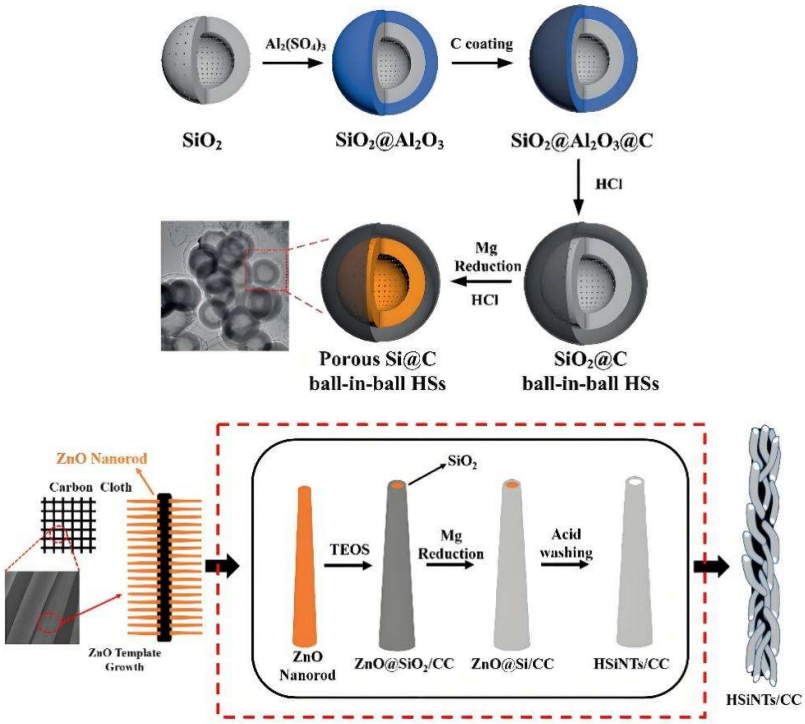

Figure 8. Schematic fabrication process of porous Si@C ball-in-ball hollow spheres[133], and the synthetic process of HSiNTs/CC by reducing silicon oxide and corroding zinc oxide nanorods templates [135].

 doi:10.20944/preprints202508.0567.v1

Silicon-carbon (Si/C) composite anode materials prepared by different methods have shown significant improvements in ICE, stability and suppression of volume expansion. Current research on Si/C composite anodes is moving towards the development of high energy density, excellent charge-discharge performance and stable cycling performance. By combining various functional carbon materials with silicon to prepare Si/C composites with different structures, while optimizing electrical conductivity, stability and cycle life, the issues such as volume expansion and particle pulverization of silicon materials are also alleviated. With further optimization of processes and improvement of designs in the future, these high-performance Si/C composite electrodes are expected to achieve more extensive commercial applications.

3.3. SiOx Anode Materials

Silicon suboxide (SiO_x)-based anode materials have emerged as representative candidates for next-generation lithium-ion battery anodes, owing to their ultra-high theoretical specific capacity, high safety and excellent rate performance. However, the low ICE remains a critical bottleneck. During lithiation and delithiation processes, SiO_x firstly reacts with Li to in-situ form elemental Si, Li_2O and lithium silicates. The elemental Si further reacts with Li to form Li_xSi alloys, contributing to reversible capacity. In contrast, the generated Li_2O and lithium silicates do not participate in subsequent electrochemical reactions [136, 137]. The particle size of the in-situ formed elemental Si is below 5 nm, with abundant interparticle voids. Meanwhile, Li_2O and lithium silicates, being inactive in subsequent cycles, exhibit no volume expansion, thereby providing additional space to buffer stress. Compared to first-generation nano-silicon materials, SiO_x has a lower theoretical specific capacity but significantly reduced volume expansion (~118%) during lithiation, leading to substantially improved cycling stability. With its high capacity and unique microstructure, SiO_x holds great potential among silicon-based anode materials. Nevertheless, the formation of large amounts of inactive substances during charge-discharge cycles results in significant irreversible capacity loss and low ICE (around 70%) [138-140]. To address this technical bottleneck, researchers have proposed strategies such as pre-lithiation and material modification to enhance the ICE of SiO_x anodes.

3.3.1. Pre-lithiation of SiO_x

Currently, pre-lithiation of silicon-based anode materials is primarily achieved through methods such as direct addition of lithium metal and lithiation additives, electrochemical pre-lithiation and chemical pre-lithiation.

The addition of metallic lithium is the most direct and effective approach to improve the ICE of anode materials. Meanwhile, small amounts of metallic lithium can mitigate capacity loss during the first charge-discharge cycle and significantly enhance battery energy density. However, excessive lithium in direct contact tends to induce lithium dendrite formation, compromising battery safety and cycling stability. To address this, Meng et al. constructed a resistance buffer layer by coating poly (vinyl butyral) on carbon nanotube films, preventing direct contact between lithium and silicon suboxide to avoid lithium dendrite growth [141]. After pre-lithiation, the ICE of the silicon suboxide material increased from 79% to 89% which retained 77% of its capacity after 200 cycles. Nevertheless, the lithiation reaction between lithium powder/foil and silicon suboxide is a solid-phase reaction, which typically requires a long time and may lead to inhomogeneity. Additionally, the high reactivity of metallic lithium demands anhydrous conditions. Excessive moisture in the air can trigger reactions producing hydrogen and heat, posing a fire hazard. Organolithium compounds, prepared via the coordination between elemental lithium and organic molecules with electron affinity in organic solvents, exhibit slightly lower reactivity than metallic lithium which enable lithiation under relatively mild conditions, significantly reducing operational risks [142-146]. When using new organolithium compounds with low redox potentials, the ICE of silicon suboxide can be increased from 61.1% to 87.1% [142]. Pre-lithiation using lithium powder/foil or organolithium compounds as lithiation agents is generally performed on the surface of prefabricated electrode sheets, which

 doi:10.20944/preprints202508.0567.v1

imposes high requirements on reaction uniformity and operating environments, hindering industrialization.

Tang et al. mixed Li_2CO_3 with SiO via ball milling followed by pre-lithiation through high-temperature treatment. Lithium ions embedded in the Si-O-Si network of the amorphous silica matrix form a lithium silicate glass-like phase, which can construct lithium-rich diffusion channels, promote the transport of lithium ions in the silica bulk and significantly enhance the electrochemical performance of the material [147]. Song et al. prepared a silica-based material involving magnesiothermic reduction of SiO_x using magnesium followed by solid-state lithiation of silica with lithium carbonate (Li_2CO_3) [148]. Magnesium can reduce silica to silicon and generate magnesium silicate, while lithium carbonate reacts with SiO_x to form lithium disilicate ($Li_2Si_2O_5$). The magnesium silicate and lithium disilicate on the surface of SiO_x can effectively alleviate the irreversible loss of lithium ions, thereby improving the ICE of SiO_x. The as-prepared SiO_x-Mg-Li_2CO_3-C nanostructure (as shown in Figure 9) shows an ultra-high ICE of 91.1% and relatively stable cycling performance. After 100 cycles at rate of 0.5 C, the capacity remains at 894.5 $mAh \cdot g^{-1}$ with retention rate of 87.9%.

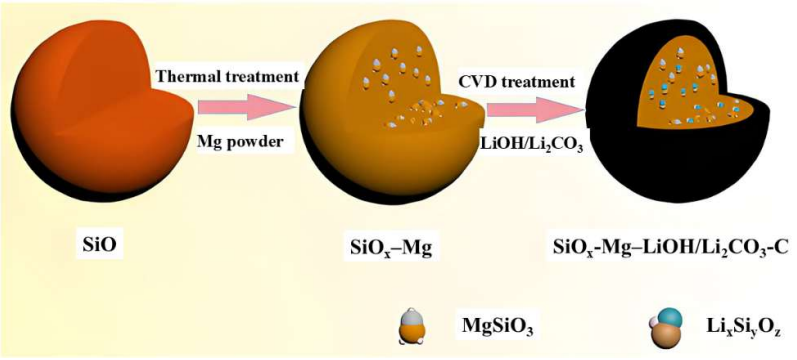

Figure 9. Schematic illustration of the synthesis process of SiO_x-Mg-Li_2CO_3/LiOH-C.[148].

The pre-lithiation by directly reacting lithium-containing solid reagents with silicon suboxide-based substances to form silicate compounds can be completed at material manufacturers, without the need to modify the battery production systems, which significantly enhances the capability of commercial promotion [149-152]. The pre-lithiated silicon suboxide-based materials with high ICE can be stored in a humidity-controlled environment, and possess good cycling stability. This solid-phase pre-lithiation featuring simple process, environmental friendliness and low safety risks has become the mainstream industrialization process for the pre-lithiation of silicon suboxide-based materials.

Electrochemical pre-lithiation is achieved by firstly fabricating SiO_x-based materials into electrode sheets, which are then assembled into cells with lithium foils. In the presence of electrolyte, lithium ions migrate from the lithium foil to the material to be pre-lithiated by controlling the current density and duration, converting silica into lithium silicate compounds [153, 154]. This process typically involves cyclic voltammetry or galvanostatic charge-discharge methods, with repeated cycling within a specific voltage range until the desired pre-lithiation degree is reached. Since this method yields pre-lithiated electrode sheets, significant technical challenges arise in subsequent processing: whether disassembling and reassembling the electrode sheets into cells or removing the active materials from the sheets for re-coating, both procedures are highly complex. Additionally, electrochemical pre-lithiation requires an extended reaction time, resulting in low production efficiency.

Furthermore, Chung et al. achieved pre-lithiation driven by lithium metal-free dehydrogenation using oxygen-free lithium compounds such as lithium hydride, converting silicon suboxide into three-dimensionally networked silicon/lithium silicate nanocomposite [149]. This material delivered a specific capacity of 1203 $mAh \cdot g^{-1}$ during the first lithiation/de-lithiation process, with the ICE significantly enhanced to 90.5%, demonstrating excellent reversibility. The improvement in initial efficiency brought by the pre-lithiation of silicon suboxide increased the energy density of the

 doi:10.20944/preprints202508.0567.v1

fabricated full cell by 50% and exhibited good cycling stability over 800 cycles. Other compounds such as Li_3N [155], LiF [156, 157] have also been applied in the pre-lithiation of SiO_x, which all improve the local environment of Si and O, enhance the ICE as well as the cycling stability.

Although the ICE of SiO_x anode materials has been improved after pre-lithiation treatment, the high cost of lithium sources leads to high costs. Moreover, the lithiated silicon suboxide-based materials contain a large amount of residual alkali, which will generate gas during subsequent battery cycling, resulting in performance degradation and potential safety hazards. Therefore, the development of new pre-lithiation methods will be a key research direction in the future.

3.3.2. Modification of SiO_x Materials

In addition to the aforementioned pre-lithiation, researchers have proposed strategies to improve the ICE from the perspective of modifying silicon-based anode materials. Extensive studies have been conducted with certain achievements. Currently, the methods mainly include surface coating modification and material composition design.

Different coating materials can promote the transport of interfacial electrons or lithium ions, reduce reactions between active materials and electrolytes to prevent excessive consumption of active lithium ions, and thus improve the ICE of silicon anode materials. To enhance the electronic conductivity of silicon anode and reduce the volume change, surface carbon coating is one of the most extensively studied technologies. After surface coating and modification with carbon materials, the electrochemical activity, lithium ion diffusion ability and coulombic efficiency of SiO_x are all improved[158-160].

Studies have shown that part of the amorphous silicon in uncoated SiO_x is oxidized, while C-SiO_x with carbon coating layer reduces contact with oxygen. The initial Coulombic efficiencies of pure SiO_x and C-SiO_x are 55% and 68%, respectively [161]. Dong et al. synthesized C/SiO_2 nanocomposites by sol-gel method, achieving uniform distribution of carbon and silica at the molecular level [159]. After carbonization at 800 °C, the C/SiO_2-800 °C nanocomposite has not only high specific surface area of 480.38 $m^2 \cdot g^{-1}$ but also promoted conductivity. These improvements significantly enhance the electrochemical activity and lithium ion diffusion ability of the material. The C/SiO_2-800 °C anode still exhibits an excellent reversible capacity of 832.19 $mAh \cdot g^{-1}$ after 300 cycles at current density of 100 $mA \cdot g^{-1}$.

Carbon materials doped with nitrogen (N) and phosphorus (P) often show more excellent electrochemical performance. As shown in Figure 10, the ICE of the SiO_x/G@CNP anode coated with N-P co-doped carbon layer after ball milling and heat treatment is significantly improved [162]. However, excessive amorphous carbon coating layer hinder the contact between SiO_x and Li+. Moreover, amorphous carbon materials have issues such as large specific surface area and low ICE, which affect the practical application of carbon-coated SiO_x materials.

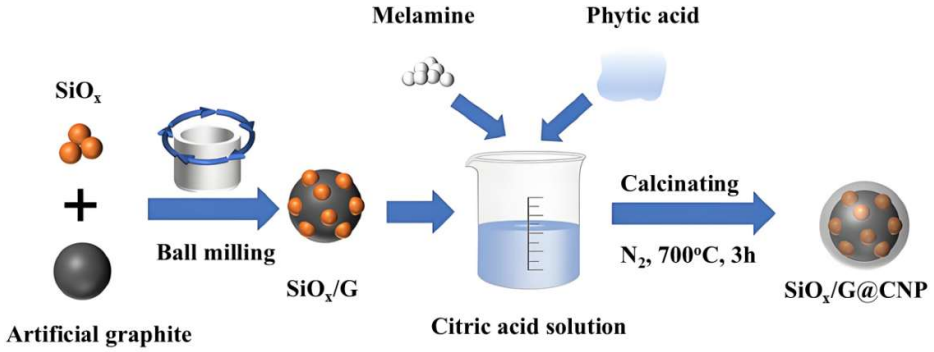

Figure 10. Schematic chart of the fabrication for SiO_x/G@CNP. [162].

In addition to surface coating and surface modification, some scholars have attempted to improve the ICE by altering the intrinsic microstructure and composition of SiO_x materials. On one

 doi:10.20944/preprints202508.0567.v1

hand, the irreversible capacity generated during the first lithiation of SiO_x materials stems from the formation of oxygen-containing inert products. Therefore, reducing the oxygen content can decrease the generation of inert products and enhance the ICE. For instance, the oxygen content in the material can be controlled through high-temperature preparation [163]. Some scholars have proposed introducing metals such as Mg [164]、Al [165]、Ag [166], Ge [167, 168], Co [169] or alloys [170, 171] to transfer oxygen elements in SiOx to the metals, forming corresponding silicates. This approach can reduce side reactions on the electrode surface, improve electrical conductivity and thereby enhance the initial efficiency, cycling stability and other electrochemical performances. Furthermore, some metal oxides, such as Al_2O_3 [172, 173], Fe_2O_3 [174], Fe_3O_4 [175] and TiO_2[176-180] , have also been used to improve the microstructure and composition of SiO_x, consequently enhancing the ICE.

On the other hand, since SiO is thermodynamically unstable, it undergoes a disproportionation reaction such as $2\ SiO \rightarrow Si + SiO_2$ under high temperature. This converts part of the oxygen in the SiO_x lattice into electrochemically inactive SiO_2 before the lithiation reaction, which can reduce the subsequent formation of lithium silicates or lithium oxides, decrease irreversible capacity and thereby improve the ICE of the material. The introduction of some metal oxides can also convert the SiO_2 component in SiO_x into silicates, promoting the occurrence of its disproportionation reaction. For example, mixing Fe_2O_3 with SiO followed by heat treatment form iron silicate (Fe_2SiO_4), which improves the ICE of the silicon suboxide anode material [181]. MgO can react with the amorphous SiO_2 in SiO_x, promoting the disproportionation of SiO and effectively reducing the subsequent reaction between active Li^+ and SiO_2. As a result, the ICE is significantly improved [182]. In addition, transition metal oxides themselves can serve as anode materials for LIBs with good reversibility during charge-discharge cycles resulting from the in-situ electrochemical size confinement effect of transition metal nanoparticles dispersed in nano-Li_2O matrix [183]. The electrochemical activity between transition metals and Li_2O greatly promotes the possibility and extent of the conversion. Meanwhile, transition metals can also improve the electrical conductivity of the material. Therefore, SiO_2 composites modified with transition metals or metal oxides show high ICE [184].

The introduction of Sn into silicon-based materials can enhance the electrochemical performance. Compared with SiO, the ICE of Sn/SiO composites increase by 20%, even exceeding 90% at voltage of 3.0 V [185]. In addition, the composite prepared by two-step ball milling of Sn-Fe alloy and SiO_x also has a much higher ICE than the matrix SiO_x. Nano-sized Sn_2Fe firmly attached to the surface of SiO_x (Figure 11), which improves the electronic conductivity of SiO_x and promotes the reversible extraction of Li+ from the Li-Si-O glass. Thus, when the introduction amount of Sn_2Fe is 70 wt%, the initial efficiency of the composite material can reach approximately 78% [186].

Figure 11. Illustration of preparation and electrochemical reaction for the Sn_2Fe@SiOx composites [186].

Furthermore, Zhou et al. synthesized a yolk-shell structured nano-spherical anode material (SiO/MWCNTs@C) [187]. Multi-walled carbon nanotubes (MWCNTs) are located between the silicon oxide (SiO) core and the outer carbon layer, functioning as a bridging component which enhances the lithium ion diffusion capability, electrical conductivity and cycling stability, thereby significantly improving the electrochemical performance for LIBs. The material exhibits an ICE of 76.18%. Even after 200 cycles at current density of 5000 $mA{\cdot}g^{-1}$, it can still maintain a reversible specific capacity of 844 $mAh{\cdot}g^{-1}$ with capacity retention rate of 92%.

 doi:10.20944/preprints202508.0567.v1

The aforementioned prelithiation methods and material modifications have improved the ICE of the active materials to some extent through composition and structural optimization. However, there remains significant room for enhancing the ICE and other electrochemical properties of silicon-based anode materials. Moreover, existing strategies for improving the ICE and cycling stability of SiO materials still face challenges such as high preparation costs, complex synthesis processes and poor product consistency. Additionally, modified materials often suffer from reduced specific capacity, inferior cycling stability and diminished rate capability, which hinder their large-scale commercialization.

4. Conclusions

In this article, the expansion mechanisms and modification strategies of silicon-based anode materials for LIBs are systematically reviewed with a focus on multidimensional nanostructured silicon, SiC composites and SiO_x anodes, aiming to address the challenges posed by silicon expansion. Simply reducing silicon to nanoscale, thin-film or porous structures does not fundamentally resolve the issue. Instead, the development of SiC composites with optimized structures and the prelithiation/modification of SiO_x are expected to be key research directions in the future.

Silicon-carbon (Si-C) anodes have emerged as a critical research direction due to the high specific capacity, enhanced safety, abundant raw materials and simple preparation processes. From a technical perspective, future advancements in Si-C anodes may include: (1) Structural optimization: Weak interfacial bonding between Si and C particles leads to detachment and capacity degradation. Novel architectures such as hollow structures, core-shell confinement or 3D interconnected buffer layers could improve mechanical stability. (2) Advanced binders: Developing elastic, adhesive, conductive, electrochemically stable and environmentally friendly binders to enhance electrochemical performance. (3) Innovative synthesis techniques: Current methods are complex. Future efforts should focus on optimizing CVD processes or other scalable techniques to improve efficiency and reduce costs. Additionally, atomic-level interfacial engineering to strengthen Si-C heterojunctions while maintaining structural integrity and high silicon loading is crucial.

Silicon monoxide (SiO_x)-based anodes, with their ultrahigh theoretical capacity, safety and rate capability, represent a promising next-generation lithium-ion battery material. However, the low ICE remains a major barrier. Future research on SiO_x anodes should prioritize on: (1) Oxygen content regulation: Introducing metals or metal oxides to adjust oxygen stoichiometry, combined with prelithiation, to optimize phase structure and enhance reversible capacity. (2) Hierarchical composite design and binders: Multiscale structural engineering (e.g. coated or cage-like porous frameworks) to mitigate pulverization, paired with high-performance binders for electrode stabilization.

As a cornerstone innovation for next-generation LIBs, silicon-based anodes are at a critical juncture where technological breakthroughs and industrial scalability converge. Accelerating the commercialization requires the development of hierarchically porous and core-shell composite materials, alongside innovations in synthesis parameter optimization, novel fabrication methods, purity control, particle size distribution tuning and surface modification techniques. These advancements will provide vital support for the large-scale adoption of silicon-based anodes.

Conflicts of Interest: The authors declare no conflicts of interest.

Abbreviations

The following abbreviations are used in this manuscript:

LIBs	Lithium-ion batteries
SEI	Solid electrolyte interphase
ICE	Initial coulombic efficiency
CVD	Chemical vapor deposition

 doi:10.20944/preprints202508.0567.v1

References

1. Li L.; Zhang X.; Li M.; Chen R.; Wu F.; Amine K.; Lu J. The recycling of spent lithium-ion batteries: a review of current processes and technologies. *Electro. Ener. Rev.* **2018**, 1, 461-482.
2. Xu J.; Cai X.; Cai S.; Shao Y.; Hu C.; Lu S.; Ding S. High-energy lithium-ion batteries: recent progress and a promising future in applications. *Energy Environ. Mater.* **2023**, 6, e12450.
3. Fang R.; Chen K.; Yin L.; Sun Z.; Li F.; Cheng H. The regulating role of carbon nanotubes and graphene in lithium-ion and lithium–sulfur batteries. *Adv. Mater.* **2019**, 31, 1800863.
4. Zhao H.; Zuo H.; Wang J.; Jiao S. Practical application of graphite in lithium-ion batteries: modification, composite, and sustainable recycling. *J. Energy Storage* **2024**, 98, 113125.
5. Peng J.; Li W.; Wu Z.; Li H.; Zeng P.; Yang J.; Hu S.; Chen G.; Chang B.; Wang X. Engineering Si-based anode materials with homogeneous distribution of SiOx and carbon for lithium-ion batteries. *Energy Fuels* **2022**, 36, 5465-5474.
6. Tao W.; Wang P.; You Y.; Park K.; Wang C.; Li Y.; Cao F.; Xin S. Strategies for improving the storage performance of silicon-based anodes in lithium-ion batteries. *Nano Res.* **2019**, 12, 1739-1749.
7. Kwon T.; Choi J. W.; Coskun A. Prospect for supramolecular chemistry in high-energy-density rechargeable batteries. *Joule* **2019**, 3 662-682.
8. Xu X.; Zhang H.; Chen Y.; Li N.; Li Y.; Liu L. SiO_2@SnO_2/graphene composite with a coating and hierarchical structure as high performance anode material for lithium ion battery. *J. Alloy. Compd.* **2016**, 677, 237-244.
9. McBrayer J. D.; Rodrigues M. T. F.; Schulze M. C.; Abraham D. P.; Apblett C. A.; Bloom I.; Carroll G. M.; Colclasure A. M.; Fang C.; Harrison K. L.; Liu G.; Minteer S. D.; Neale N. R.; Veith G. M.; Johnson C. S.; Vaughey J. T.; Burrell A. K.; Cunningham B. Calendar aging of silicon-containing batteries. *Nat. Energy* **2021**, 6, 866-872.
10. Sunghun Choi T. K.; Coskun A.; Choi J. W. Highly elastic binders integrating polyrotaxanes for silicon microparticle anodes in lithium ion batteries. *Science* **2017**, 357 279–283.
11. Wang C.; Wen J.; Luo F.; Quan B.; Li H.; Wei Y.; Gu C.; Li J. Anisotropic expansion and size-dependent fracture of silicon nanotubes during lithiation. *J. Mater. Chem. A* **2019**, 7 15113-15122.
12. Pan H.; Wang L.; Shi Y.; Sheng C.; Yang S.; He P.; Zhou H. A solid-state lithium-ion battery with micron-sized silicon anode operating free from external pressure. Nat. Commun. 2024, 15, 2263.
13. Kang W.; Zhang Q.; Jia Y.; Liu X.; Jiang N.; Zhao Y.; Wu C.; Guan L. Enhancing the cycling stability of commercial silicon nanoparticles by carbon coating and thin layered single-walled carbon nanotube webbing. *J. Power Sources* **2024**, 602, 234338.
14. Huo H.; Jiang M.; Bai Y.; Ahmed S.; Volz K.; Hartmann H.; Henss A.; Singh C.V.; Raabe D.; Janek J. Chemo-mechanical failure mechanisms of the silicon anode in solid-state batteries. *Nat. Mater.* **2024**, 23, 543-551.
15. Zhu X.; Meng F.; Zhang Q.; Xue L.; Zhu H.; Lan S.; Liu Q.; Zhao J.; Zhuang Y.; Guo Q.; Liu B.; Gu L.; Lu X.; Ren Y.; Xia H. $LiMnO_2$ cathode stabilized by interfacial orbital ordering for sustainable lithium-ion batteries. *Nat. Sustain.* **2021**, 4, 392-401.
16. Manthiram A. A reflection on lithium-ion battery cathode chemistry. *Nat. Commun.* **2020**, 11, 1550.
17. Hou X.; Liu X.; Wang H.; Zhang X.; Zhou J.; Wang M. Specific countermeasures to intrinsic capacity decline issues and future direction of $LiMn_2O_4$ cathode. *Energy Storage Mater.* **2023**, 57, 577-606.
18. Lee S.; Su L.; Mesnier A.; Cui Z.; Manthiram A.; Cracking vs. surface reactivity in high-nickel cathodes for lithium-ion batteries. *Joule* **2023**, 7, 2430-2444.
19. Chen S.; Lv D.; Chen J.; Zhang Y.; Shi F. Review on defects and modification methods of $LiFePO_4$ cathode material for lithium-ion batteries. *Energ. Fuel.* **2022**, 36, 1232-1251.
20. Ling J.; Karuppiah C.; Krishnan S. G.; Reddy M. V.; Misnon I. I.; Ab Rahim M. H.; Yang C. C.; Jose R. Phosphate polyanion materials as high-voltage lithium-ion battery cathode: a review. *Energ. Fuel.* **2021**, 35, 10428-10450.
21. Wani T. A.; Suresh G. A comprehensive review of $LiMnPO_4$ based cathode materials for lithium-ion batteries: current strategies to improve its performance. *J. Energy Storage* **2021**, 44, 103307.

 doi:10.20944/preprints202508.0567.v1

22. Ge M.; Cao C.; Biesold G.M.; Sewell C.D.; Hao S.M., Huang J.; Zhang W.; Lai Y.; Lin Z. Recent advances in silicon-based electrodes: from fundamental research toward practical applications. *Adv. Mater.* **2021**, 33, 2004577.
23. Divakaran A.M.; Minakshi M.; Bahri P.A.; Paul S.; Kumari P.; Divakaran A.M.; Manjunatha K.N. Rational design on materials for developing next generation lithium-ion secondary battery. *Prog. Solid State Ch.* **2021**, 62, 100298.
24. Xu Z. L.; Liu X.; Luo Y.; Zhou L.; Kim J.-K. Nanosilicon anodes for high performance rechargeable batteries. *Prog. Mater. Sci.* **2017**, 90, 1-44.
25. Lin M. C.; Gong M.; Lu B.; Wu Y.; Wang D. Y.; Guan M.; Angell M.; Chen C.; Yang J.; Hwang B.-J.; Dai H. An ultrafast rechargeable aluminium-ion battery. *Nature* **2015**, 520, 324-328.
26. Zhang H.; Li C.; Eshetu G. G.; Laruelle S.; Grugeon S.; Zaghib K.; Julien C.; Mauger A.; Guyomard D.; Rojo T.; Gisbert-Trejo N.; Passerini S.; Huang X.; Zhou Z.; Johansson P.; Forsyth M. From solid-solution electrodes and the rocking-chair concept to today's batteries. *Angew. Chem. Int. Ed.* **2019**, 59, 534-538.
27. Huggins R.A. Lithium alloy negative electrodes. *J. Power Sources* **1999**, 81-82, 13-19.
28. Johari P.; Qi Y.; Shenoy V. B. The mixing mechanism during lithiation of Si negative electrode in Li-ion batteries: an ab initio molecular dynamics study. *Nano Lett.* **2011**, 11, 5494-5500.
29. Wu H.; Cui Y. Designing nanostructured Si anodes for high energy lithium ion batteries. *Nano Today* **2012**, 7, 414-429.
30. Hossain M.A.M.; Hannan M.A.; Ker P.J.; Tiong S.K.; Salam M.A.; Abdillah M.; Mahlia T.M.I. Silicon-based nanosphere anodes for lithium-ion batteries: Features, progress, effectiveness, challenges, and prospects. *J. Energy Storage* **2024**, 99, 113371.
31. Wang L.; Yu J.; Li S.; Xi F.; Ma W.; Wei K.; Lu J.; Tong Z.; Liu B.; Luo B. Recent advances in interface engineering of silicon anodes for enhanced lithium-ion battery performance. *Energy Storage Mater.* **2024**, 66, 103243.
32. Obrovac M.N.; Christensen L. Structural changes in silicon anodes during lithium insertion extraction. *Electrochem. Solid-State Lett.* **2004**, 7, A93-A96.
33. Limthongkul P.; Jang Y.-I.; Dudney N.J.; Chiang Y.-M. Electrochemically-driven solid-state amorphization in lithium-silicon alloys and implications for lithium storage. *Acta Mater.* **2003**, 51, 1103-1113.
34. Obrovac M. N.; Krause L. J. Reversible cycling of crystalline silicon powder. *J. Electrochem. Soc.* **2007**, 154, A103-A108.
35. Zhao X.; Lehto V.-P. Challenges and prospects of nanosized silicon anodes in lithium-ion batteries. *Nanotechnology* **2020**, 32, 042002.
36. Chan K.S.; Liang W.-W.; Chan C.K. First-principles studies of the lithiation and delithiation paths in Si anodes in Li-ion batteries. *J. Phys. Chem. C* **2019**, 123, 22775-22786.
37. Limthongkul P.; Jang Y.-I.; Dudney N.J.; Chiang Y.-M. Electrochemically-driven solid-state amorphization in lithium–metal anodes. *J. Power Sources* **2003**, 119-121, 604-609.
38. Liu X.H.; Wang J.W.; Huang S.; Fan F.; Huang X.; Liu Y.; Krylyuk S.; Yoo J.; Dayeh S.A.; Davydov A.V.; Mao S.X.; Picraux S.T.; Zhang S.; Li J.; Zhu T.; Huang J.Y. In situ atomic-scale imaging of electrochemical lithiation in silicon. *Nat. Nanotechnol.* **2012**, 7, 749-756.
39. Baris Key R.B.; Morcrette M.; Seznéc V.; Tarascon J.-M.; Grey C. P. Real-time NMR investigations of structural changes in silicon electrodes for lithium-ion batteries. *J. Am. Chem. Soc.* **2009**, 131, 9239–9249.
40. McDowell M.T.; Lee S.W.; Nix W.D.; Cui Y. 25th Anniversary article: Understanding the lithiation of silicon and other alloying anodes for lithium-ion batteries. *Adv. Mater.* **2013**, 25, 4966-4985.
41. Gu M.; He Y.; Zheng J.; Wang C.; Nanoscale silicon as anode for Li-ion batteries: The fundamentals, promises, and challenges. *Nano Energy* **2015**, 17, 366-383.
42. Ding N.; Xu J.; Yao Y.X.; Wegner G.; Fang X.; Chen C.H.; Lieberwirth I. Determination of the diffusion coefficient of lithium ions in nano-Si. *Solid State Ionics* **2009**, 180, 222-225.
43. Bordes A.; De Vito E.; Haon C.; Boulineau A.; Montani A.; Marcus P. Multiscale investigation of silicon anode Li insertion mechanisms by Time-of-Flight secondary ion mass spectrometer imaging performed on an in situ focused ion beam cross section. *Chem. Mater.* **2016**, 28, 1566-1573.

 doi:10.20944/preprints202508.0567.v1

44. Gu M.; Wang Z.; Connell J. G.; Perea D. E.; Lauhon L. J.; Gao F.; Wang C. Electronic origin for the phase transition from amorphous LixSi to crystalline $Li_{15}Si_4$. *ACS Nano* **2013**, 7, 6303–6309.
45. Wang C.; Li X.; Wang Z.; Xu W.; Liu J.; Gao F.; Kovarik L.; Zhang J.; Howe J.; Burton D.J.; Liu Z.; Xiao X.; Thevuthasan S.; Baer D.R. In Situ TEM investigation of congruent phase transition and structural evolution of nanostructured silicon/carbon anode for lithium ion batteries. *Nano Lett.* **2012**, 12, 1624-1632.
46. Liu X.; Zheng H.; Zhong L.; Huang S.; Karki K.; Zhang L., Liu Y.; Kushima A.; Liang W.; Wang J.; Cho J.-H.; Epstein E.; Dayeh S. A.; Picraux S.T.; Zhu T.; Li J.; Sullivan J.P.; Cumings J.; Wang C.; Mao S.; Ye Z.; Zhang S.; Huang J. Anisotropic swelling and fracture of silicon nanowires during lithiation. *Nano Lett*. **2011**, 11, 3312-3318.
47. Liu X.; Zhang L.; Zhong L.; Liu Y.; Zheng H.; Wang J.; Cho J.-H.; Dayeh S.A.; Picraux S.T.; Sullivan J.P.; Mao S.; Ye Z.; Huang J. Ultrafast electrochemical lithiation of individual Si nanowire anodes. *Nano Lett.* **2011**, 11, 2251-2258.
48. Kang Y.-M.; Lee S.-M.; Kim S.-J.; Jeong G.-J.; Sung M.-S.; Choi W.-U.; Kim S.-S. Phase transitions explanatory of the electrochemical degradation mechanism of Si based materials. *Electrochem. Commun.* **2007**, 9, 959-964.
49. Sumohan Misra N.L.; Nelson J.; Sae Hong S.; Cui Y.; Toney M. F. In situ X-ray diffraction studies of (De)lithiation mechanism in silicon nanowire anodes. *ACS Nano* **2012**, 6, 5465–5473.
50. McDowell M.T.; Lee S.W.; Harris J.T.; Korgel B.A.; Wang C.; Nix W.D.; Cui Y. In situ TEM of two-phase lithiation of amorphous silicon nanospheres. *Nano Lett.* **2013**, 13, 758-764.
51. Baris Key M.M.; Tarascon J.-M.; Grey C. P. Pair distribution function analysis and solid state NMR studies of silicon electrodes for lithium ion batteries Understanding the (de)lithiation mechanisms. *J. Am. Chem. Soc.* **2011**, 133, 503–512.
52. Li Y.; Li Q.; Chai J.; Wang Y.; Du J.; Chen Z.; Rui Y.; Jiang L.; Tang B. Si-based anode lithium-ion batteries: a comprehensive review of recent progress. *ACS Mater. Lett.* **2023**, 5, 2948-2970.
53. Liu X.; Zhong L.; Huang S.; Mao S. X.; Zhu T.; Huang J. Size-dependent fracture of silicon nanoparticles during lithiation. *ACS Nano* **2012**, 6, 1522–1531.
54. Wu X.; Pan K.; Jia M.; Ren Y.; He H.; Zhang L.; Zhang S. Electrolyte for lithium protection: From liquid to solid. *Green Energy Environ.* **2019**, 4, 360-374.
55. Dupré N.; Moreau P.; De Vito E.; Quazuguel L.; Boniface M.; Bordes A.; Rudisch C.; Bayle-Guillemaud P.; Guyomard D. Multiprobe study of the solid electrolyte interphase on silicon-based electrodes in full-cell configuration. *Chem. Mater.* **2016**, 28, 2557-2572.
56. Huang J.; Liu X.; Liu Y.; Kushima A.; Li J.; Zhu T. In-situ TEM experiments of electrochemical lithiation and delithiation of individual nanostructures. *Microsc. Microanal.* **2012**, 18, 1326-1327.
57. Luo F.; Liu B.; Zheng J.; Chu G.; Zhong K.; Li H.; Huang X.; Chen L. Review-nano-silicon carbon composite anode materials towards practical application for next generation Li-ion batteries. *J. Electrochem. Soc.* **2015**, 162, A2509-A2528.
58. Xu C.; Lindgren F.; Philippe B.; Gorgoi M.; Björefors F.; Edström K.; Gustafsson T. Improved performance of the silicon anode for Li-ion batteries: Understanding the surface modification mechanism of fluoroethylene carbonate as an effective electrolyte additive. *Chem. Mater.* **2015**, 27, 2591-2599.
59. Luo W.; Chen X.; Xia Y.; Chen M.; Wang L.; Wang Q.; Li W.; Yang J. Surface and interface engineering of silicon-based anode materials for lithium-ion batteries. *Adv. Energy Mater.* **2017**, 7 1701083.
60. Fan S.; Wang H.; Qian J.; Cao Y. ; Yang H.; Ai X. ; Zhong F. Covalently bonded silicon/carbon nanocomposites as cycle-stable anodes for Li-ion batteries. *ACS Appl. Mater. Inter.* **2020,** 12, 16411-16416.
61. Li Y.; Lv L.; Huang W. ; Zhu Y.; Long F.; Zheng W.; Qu Q.; Zheng H. In situ polymerized and imidized Si@Polyimide microcapsules with flexible solid-electrolyte interphase and enhanced electrochemical activity for Li-storage. *ChemElectroChem* **2022**, 9, e202101409.

 doi:10.20944/preprints202508.0567.v1

62. An W.; He P.; Che Z.; Xiao C.; Guo E.; Pang C.; He X.; Ren J.; Yuan G.; Du N.; Yang D.; Peng D.-L.; Zhang Q. Scalable synthesis of pore-rich Si/C@C core–shell-structured microspheres for practical long-life Lithium-ion battery anodes. ACS *Appl. Mater. Inter.* **2022**, 14, 10308-10318.
63. Mu G.; Ding Z.; Mu D.; Wu B.; Bi J.; Zhang L.; Yang H.; Wu H.; Wu F. Hierarchical void structured Si/PANi/C hybrid anode material for high-performance lithium-ion batteries. *Electroch. Acta* **2019**, 300, 341-348.
64. Lu J.; Liu J.; Gong X.; Wang Z. Fe3C doped modified nano-Si/C composites as high-coulombic-efficiency anodes for lithium-ion batteries. *Sustain. Energ. Fuels* **2021**, 5, 6170-6180.
65. Yao Y.; McDowell M.T.; Ryu I.; Wu H.; Liu N.; Hu L.; Nix W. D.; Cui Y. Interconnected silicon hollow nanospheres for lithium-ion battery anodes with long cycle life. *Nano Lett.* **2011**, 11, 2949-2954.
66. Ge M.; Rong J.; Fang X.; Zhang A.; Lu Y.; Zhou C. Scalable preparation of porous silicon nanoparticles and their application for lithium-ion battery anodes, *Nano Res.* **2013**, 6, 174-181.
67. Yang Y.; Wu S.; Chiu H.; Lin P.; Chen Y. Catalytic growth of silicon nanowires assisted by laser ablation, *J. Phys. Chem. B* **2004**, 108 846-852.
68. Chan C.K.; Peng H.; Liu G.; McIlwrath K.; Zhang X. F.; Huggins R.A.; Cui Y. High-performance lithium battery anodes using silicon nanowires. *Nat. Nanotechnol.* **2008**, 3, 31-35.
69. Ortaboy S.; Alper J. P.; Rossi F.; Bertoni G.; Salviati G.; Carraro C.; Maboudian R. MnOx-decorated carbonized porous silicon nanowire electrodes for high performance supercapacitors. *Energy Environ. Sci.* **2017**, 10, 1505-1516.
70. Lu J.; Liu J.; Gong X.; Pang S.; Zhou C.; Li H.; Qian G.; Wang Z. Upcycling of photovoltaic silicon waste into ultrahigh areal-loaded silicon nanowire electrodes through electrothermal shock. *Energy Storage Mater.* **2022**, 46, 594-604.
71. Lu Z.; Wong T.; Ng T.-W.; Wang C. Facile synthesis of carbon decorated silicon nanotube arrays as anode material for high-performance lithium-ion batteries. *RSC Adv.* **2014**, 4, 2440-2446.
72. Tong L.; Wang P.; Chen A.; Qiu F.; Fang W.; Yang J.; Wang C.; Yang Y. Improved electrochemical performance of binder-free multi-layered silicon/carbon thin film electrode for lithium-ion batteries. *Carbon* **2019**, 153, 592-601.
73. Liao L.; Ma T.; Xiao Y.; Wang M.; Cao Y.; Fang T. Enhanced reversibility and cyclic stability of biomass-derived silicon/carbon anode material for lithium-ion battery. *J Alloy. Compd.* **2021**, 873, 159700.
74. Hwang T.H.; Lee Y.M.; Kong B.-S.; Seo J.-S.; Choi J.W. Electrospun core–shell fibers for robust silicon nanoparticle-based lithium ion battery anodes. *Nano Lett.* **2012**, 12, 802-807.
75. Liu R.; Shen C.; Dong Y.; Qin J.;Wang Q.; Iocozzia J.; Zhao S.; Yuan K.; Han C.; Li B.; Lin Z. Sandwich-like CNTs/Si/C nanotubes as high performance anode materials for lithium-ion batteries. *J. Mater. Chem. A* **2018**, 6, 14797-14804.
76. Imtiaz S.; Amiinu I.S.; Storan D.; Kapuria N.; Geaney H.; Kennedy T.; Ryan K.M. Dense silicon nanowire networks grown on a stainless-steel fiber cloth: A flexible and robust anode for lithium-ion batteries. *Adv. Mater.* **2021**, 33, 2105917.
77. Farooq U.; Choi J.-H.; Kim D.; Pervez S.A.; Yaqub A.; Hwang M.-J.; Lee Y.-J.; Lee W.-J.; Choi H.-Y.; Lee S.-H.; You J.-H.; Ha C.-W.; Doh C.-H. Electrically exploded silicon/carbon nanocomposite as anode material for Lithium-ion batteries. *J. Nanosci. Nanotechnol*. **2014**, 14, 9340-9345.
78. Demirkan M.T.; Trahey L.; Karabacak T. Cycling performance of density modulated multilayer silicon thin film anodes in Li-ion batteries. *J. Power Sources* **2015**, 273, 52-61.
79. Biserni E.; Xie M.; Brescia R.; Scarpellini A.; Hashempour M.; Movahed P.; George S.M.; M., Bestetti A.; Bassi L.; Bruno P. Silicon algae with carbon topping as thin-film anodes for lithium-ion microbatteries by a two-step facile method. *J. Power Sources* **2015**, 274, 252-259.
80. Cheng H.; Xiao R.; Bian H.; Li Z.; Zhan Y.; Tsang C.K.; Chung C.Y.; Lu Z.; Li Y. Periodic porous silicon thin films with interconnected channels as durable anode materials for lithium ion batteries. *Mater. Chem. Phy.* **2014**, 144, 25-30.
81. Jiang Z.; Li C.; Hao S.; Zhu K.; Zhang P. An easy way for preparing high performance porous silicon powder by acid etching Al–Si alloy powder for lithium ion battery. *Electroch. Acta* **2014**, 115, 393-398.

 doi:10.20944/preprints202508.0567.v1

82. Li X.; Gu M.; Hu S.; Kennard R.; Yan P.; Chen X.; Wang C.; Sailor M.J.; Zhang J.; Liu J. Mesoporous silicon sponge as an anti-pulverization structure for high-performance lithium-ion battery anodes. *Nat. Commun.* **2014**, 5, 4105.
83. Ge M.; Lu Y.; Ercius P.; Rong J.; Fang X.; Mecklenburg M.; Zhou C. Large-scale fabrication, 3D tomography, and lithium-ion battery application of porous silicon. *Nano Lett.* **2014**, 14, 261-268.
84. Yu Y.; Gu L.; Zhu C.; Tsukimoto S.; Van Aken P.A.; Maier J. Reversible storage of lithium in silver-coated three-dimensional macroporous silicon. *Adv. Mater.* **2010**, 22, 2247-2250.
85. Borchers A.; Pieler T. Programming pluripotent precursor cells derived from Xenopus embryos to generate specific tissues and organs. *Genes (Basel)* **2010**, 1, 413-426.
86. Ahad S.A.; Kennedy T.; Geaney H. Si nanowires: From model system to practical li-ion anode material and beyond. *ACS Energy Lett.* **2024**, 9, 1548-1561.
87. Saana A. I.; Imtiaz S.; Geaney H.; Kennedy T.; Kapuria N.; Singh S.; Ryan K.M. A thin Si nanowire network anode for high volumetric capacity and long-life lithium-ion batteries. *J. Energy Chem.* **2023**, 81, 20-27.
88. Collins G.A.; Kilian S.; Geaney H.; Ryan K. M. A nanowire nest structure comprising copper silicide and silicon nanowires for Lithium-ion battery anodes with high areal loading. *Small* **2021**, 17, 2102333.
89. Park Mi-H.; Kim M.G.; Joo J.; Kim K.; Kim J.; Ahn S.; Cui Y.; Cho J. Silicon nanotube battery anodes. *Nano Lett.* **2009**, 9, 3844-3847.
90. Jeong Y. K.; Huang W.; Vilá R.A.; Huang W.; Wang J.; Kim S.C.; Kim Y. S.; Zhao J.; Cui Y. Microclusters of kinked silicon nanowires synthesized by a recyclable iodide process for high-performance lithium-ion battery anodes. *Adv. Energy Mater.* **2020**, 10, 2002108.
91. Yang Y.; Yuan W.; Kang W.; Ye Y.; Pan Q.; Zhang X.; Ke Y.; Wang C.; Qiu Z.; Tang Y. A review on silicon nanowire-based anodes for next-generation high-performance lithium-ion batteries from a material-based perspective. *Sustain. Energy Fuels* **2020**, 4, 1577-1594.
92. Wu H.; Chan G.; Choi J. W.; Ryu I.; Yao Y.; McDowell M.T.; Lee S.W.; Jackson A.; Yang Y.; Hu L.; Cui Y. Stable cycling of double-walled silicon nanotube battery anodes through solid-electrolyte interphase control. *Nat. Nanotechnol.* **2012**, 7, 310-315.
93. Maranchi J. P.; Hepp A. F.; Kumtaa P. N. High capacity, reversible silicon thin-film anodes for lithium-ion batteries. Electrochem. *Solid State Lett.* **2003**, 6, A198-A201.
94. Bourderau S.; Brousse T.; Schleich D. M. Amorphous silicon as a possible anode material for Li-ion batteries. *J. Power Sources* **1999**, 81-82, 233-236.
95. J. Li, Dozier A.K.; Li Y.; Yang F.; Cheng Y.-T. Crack pattern formation in thin film lithium-ion battery electrodes. *J Electrochem. Soc.* **2011**, 158, A689.
96. Yu C.; Li X.; Ma T.; Rong J.; Zhang R.; Shaffer J.; An Y.; Liu Q.; Wei B.; Jiang H. Silicon thin films as anodes for high-performance Lithium-ion batteries with effective stress relaxation. *Adv. Energy Mater.* **2012**, 2, 68-73.
97. Elomari G.; Larhlimi H.; Oubaki R.; Elmaataouy E.; Aqil M.; Samih Y.; Makha M.; Negrila C.; Alami J.; Dahbi M. Fast charging and high-efficiency sputter-deposited silicon thin film anodes for Li-ion batteries. *J. Power Sources* **2025**, 642, 236967.
98. Liu N.; Lu Z.; Zhao J.; McDowell M.T.; Lee H.-W.; Zhao W.; Cui Y. A pomegranate-inspired nanoscale design for large-volume-change lithium battery anodes. *Nat. Nanotechnol.* **2014**, 9, 187-192.
99. Li Y.; Yan K.; Lee H.-W.; Lu Z.; Liu N.; Cui Y. Growth of conformal graphene cages on micrometre-sized silicon particles as stable battery anodes. *Nat. Energy* **2016**, 1, 15029.
100. Wang J.; Liao L.; Li Y.; Zhao J.; Shi F.; Yan K.; Pei A.; Chen G.; Li G.; Lu Z.; Cui Y. Shell-protective secondary silicon nanostructures as pressure-resistant high-volumetric-capacity anodes for Lithium-ion batteries. *Nano Lett.* **2018**, 18, 7060-7065.
101. Ko M.; Chae S.; Jeong S.; Oh P.; Cho J. Elastic a-silicon nanoparticle backboned graphene hybrid as a self-compacting anode for high-rate Lithium ion batteries. *ACS Nano* **2014**, 8, 8591-8599.
102. An Y.; Tian Y.; Zhang Y.; Wei C.; Tan L.; Zhang C.; Cui N.; Xiong S.; Feng J.; Qian Y. Two-dimensional silicon/carbon from commercial alloy and CO_2 for Lithium storage and flexible $Ti_3C_2T_x$ MXene-based Lithium–metal batteries. *ACS Nano* **2020**, 14, 17574-17588.

 doi:10.20944/preprints202508.0567.v1

103. Zhang Z. D.; Zhou H.P.; Feng T.T.; Zhao R.; Wang Y.; He M.; Xu Z.Q.; Liao J.X.; Xue W.D.; Wu M.Q. A plasma strategy for high-quality Si/C composite anode: From tailoring the current collector to preparing the active materials. *Electroch. Acta* **2020**, 347, 136222.
104. Zhang Z. D.; Zhou H.P.; Xue W.D.; Zhao R.; Wang W.J.; Feng T.T.; Xu Z.Q.; Zhang S.; Liao J.X.; Wu M.Q. Nitrogen-plasma doping of carbon film for a high-quality layered Si/C composite anode. *J. Colloid Interface Sci.* **2022**, 605, 463-471.
105. Li X.; Wu M.; Feng T.; Xu Z.; Qin J.; Chen C.; Tu C.; Wang D. Graphene enhanced silicon/carbon composite as anode for high performance lithium-ion batteries. *RSC Adv.* **2017**, 7, 48286-48293.
106. Qin J.; Wu M.; Feng T.; Chen C.; Tu C.; Li X.; Duan C.; Xia D.; Wang D. High rate capability and long cycling life of graphene-coated silicon composite anodes for lithium ion batteries. *Electroch. Acta* **2017**, 256, 259-266.
107. Wang R.; Cao J.; Xu C.; Wu N.; Zhang S.; Wu M. Low-temperature electrolytes based on linear carboxylic ester co-solvents for SiO(x)/graphite composite anodes. *RSC Adv.* **2023**, 13; 13365-13373.
108. Wang W.; Kumta P. N. Nanostructured hybrid silicon-carbon nanotube heterostructures reversible high-capacity Lithium-ion anodes. *ACS Nano* **2010**, 4, 2233-2241.
109. Tao H.; Xiong L.; Zhu S.; Zhang L.; Yang X. Porous Si/C/reduced graphene oxide microspheres by spray drying as anode for Li-ion batteries. *J. Electroanal. Chem.* **2017**, 797,16-22.
110. Zhang J.; Chen Y.; Chen X.; Feng T.; Yang P.; An M. Preparation of graphene-like carbon attached porous silicon anode by magnesiothermic and nickel-catalyzed reduction reactions. *Ionics* **2020**, 26, 5941-5950.
111. Cabello M.; Gucciardi E.; Herrán A.; Carriazo D.; Villaverde A.; Rojo T. Towards a high-power Si@graphite anode for Lithium ion batteries through a wet ball milling process. *Molecules* **2020**, 25 2494.
112. Wan W.; Mai Y.; Guo D.; Hou G.; Dai X.; Gu Y.; Li S.; Wu F. A novel sol-gel process to encapsulate micron silicon with a uniformly Ni-doped graphite carbon layer by coupling for use in lithium ion batteries. *Synthetic Met.* **2021**, 274, 116717.
113. Azam M.A.; Safie N.E.; Ahmad A.S.; Yuza N.A.; Zulkifli N.S.A. Recent advances of silicon, carbon composites and tin oxide as new anode materials for lithium-ion battery: A comprehensive review. *J. Energy Storage* **2021**, 33, 102096.
114. Wang C. S.; Wu G.T.; Zhang X. B.; Qi Z. F.; Li W. Z. Lithium insertion in carbon-silicon composite materials produced by mechanical milling. *J. Electrochem. Soc.* **1998**, 145, 2751-2758.
115. He S.; Huang S.; Wang S.; Mizota I.; Liu X.; Hou X. Considering critical factors of Silicon/Graphite anode materials for practical high-energy Lithium-ion battery applications. *Energy Fuels* **2020**, 35, 944-964.
116. Li Z.; Wan Z.; Zeng X.; Zhang S.; Yan L.; Li J.; Wang H.; Ma Q.; Liu T.; Lin Z.; Ling M.; Liang C. A robust network binder via localized linking by small molecules for high-areal-capacity silicon anodes in lithium-ion batteries. *Nano Energy* **2021**, 79,105430.
117. Li Z.; Li D.; Sun X.; Xue Y.; Shi Y.; Fu Y.; Luo C.; Lin Q.; Gui X.; Xu K. Ion-conductive and mechanically robust chitosan-based network binder for silicon/graphite anode. *J. Energy Storage* **2024**, 93, 112264.
118. Wang X.; Li T.; Liang N.; Liu X.; Zhang F.; Li Y.; Yang Y.; Yang Y.; Ma W.; Wang Z.; Yin J.; Yang Y.; Yang L. Lithium borate/boric acid optimized multifunctional binder facilitates silicon anodes with enhanced initial coulombic efficiency, structural strength, and cycling stability. *Battery Energy* **2025**, 4, e70003.
119. Wang W.; Li X.; Chen X.; Sun M.; Wang G. Aqueous binder with self-emulsifying characteristics for practical Si/C anode in Lithium-ion batteries. *Chemistry* **2025**, 31, e202403924.
120. Yan W.; Ma S.; Su Y.; Song T.; Lu Y.; Chen L.; Huang Q.; Guan Y.; Wu F.; Li N. "Shooting three birds with one stone": Bi-conductive and robust binder enabling low-cost micro-silicon anodes for high-rate and long-cycling operation. *Energy Storage Mater.* **2025**, 76, 104140.
121. Zhang Y.-T.; Xue J.-X.; Wang R.; Jia S.-X.; Zhou J.-J.; Li L. Cross-linkable binder for composite silicon-graphite anodes in lithium-ion batteries. *Giant* **2024**, 19, 100319.

 doi:10.20944/preprints202508.0567.v1

122. Yi S.; Yan Z.; Li X.; Wang Z.; Ning P.; Zhang J.; Huang J.; Yang D.; Du N. Design of phosphorus-doped porous hard carbon/Si anode with enhanced Li-ion kinetics for high-energy and high-power Li-ion batteries. *Chem.Eng. J.* **2023**, 473, 145161.
123. Liu C.; Zhou H.P.; Zhou H.; Yang B.; Li Z.K.; Zhang S.; Feng T.T.; Xu Z.Q.;Fang Z.X.; Wu M.Q. Highly Si loading on three-dimensional carbon skeleton via CVD method for a stable Si C composite anode. *J. Energy Storage* **2025,** 116, 116083.
124. Ahn W.J.; Park B.H.; Seo S.W.; Kim S.; Im J.S. Designing of 3D porous silicon/carbon complex anode based on metal-organic frameworks for lithium-ion battery. *Carbon Lett.* **2023**, 33, 2349-2361.
125. Li X.; Li K.; Yuan L.; Han Z.; Yan Z.; Xu X.; Tang K. Cost-effective preparation of high-performance Si@C anode for lithium-ion batteries. *J. Appl. Electrochem*. **2024**, 54, 2683-2697.
126. Xu Q.; Li J.Y.; Sun J.K.; Yin Y.X.; Wan L.J.; Guo Y.G. Watermelon-inspired Si/C microspheres with hierarchical buffer structures for densely compacted Lithium-ion battery anodes. *Adv. Energy Mater.* **2016**, 7, 1601481.
127. Wei K.; Zhou L.; Wang S.; Wei J.; Yan D.; Cheng Y.; Yu Z. Watermelon-like texture lithium titanate and silicon composite films as anodes for lithium-ion battery with high capacity and long cycle life. *J. Alloy. Compd.* **2021**, 885, 160994.
128. Ashraf H.; Karahan B.D.; Biowaste valorization into valuable nanomaterials: Synthesis of green carbon nanodots and anode material for lithium-ion batteries from watermelon seeds. *Mater. Res. Bull.* **2024**, 169, 112492.
129. Ding N.; Chen Y.; Li R.; Chen J.; Wang C.; Li Z.; Zhong S. Pomegranate structured C@pSi/rGO composite as high performance anode materials of lithium-ion batteries. *Electrochim. Acta* **2021**, 367, 137491.
130. Li P.; Miao C.; Yi D.; Wei Y.; Chen T.; Wu W. Pomegranate like silicon-carbon composites prepared from lignin-derived phenolic resins as anode materials for lithium-ion batteries. *New J. Chem.* **2023**, 47, 16855-16863.
131. Di F.; Wang Z.; Ge C.; Li L.; Geng X.; Sun C.; Yang H.; Zhou W.; Ju D.; An B.; Li F. Hierarchical pomegranate-structure design enables stress management for volume release of Si anode. *J. Mater. Sci. Technol.* **2023**, 157, 1-10.
132. Hu L.; Luo B.; Wu C.; Hu P.; Wang L.; Zhang H. Yolk-shell Si/C composites with multiple Si nanoparticles encapsulated into double carbon shells as lithium-ion battery anodes. *J. Energy Chem.* **2019**, 32, 124-130.
133. Li B.; Li S.; Jin Y.; Zai J.; Chen M.; Nazakat A.; Zhan P.; Huang Y.; Qian X. Porous Si@C ball-in-ball hollow spheres for lithium-ion capacitors with improved energy and power densities. *J. Mater. Chem. A* **2018**, 6, 21098-21103.
134. Tian H.; TIan H.; Yang W.; Zhang F.; Yang W.; Zhang Q.; Wang Y.; Liu J.; Silva S.R.P.; Liu H.; Wang G. Stable hollow-structured silicon suboxide-based anodes toward high-performance Lithium-ion batteries. *Adv. Funct. Mater.* **2021**, 31, 2101796.
135. Liu H.; Chen Y.; Jiang B.; Zhao Y.; Guo X.; Ma T. Hollow-structure engineering of a silicon–carbon anode for ultra-stable lithium-ion batteries. *Dalton Trans.* **2020**, 49, 5669-5676.
136. Li Z.; Du M.; Guo X.; Zhang D.; Wang Q.; Sun H.; Wang B.; Wu Y. A. Research progress of SiO -based anode materials for lithium-ion batteries. *Chem. Eng. J.* **2023**, 473, 145294.
137. Wu J.; Dong Q.; Zhang Q.; Xu Y.; Zeng X.; Yuan Y.; Lu J. Fundamental understanding of the low Initial coulombic efficiency in SiOx anode for Lithium-ion batteries: Mechanisms and solutions. *Adv. Mater.* **2024**, 36, 2405751.
138. Zhou H.P.; Yang B.; Zhang Z.D.; Zhang H.; Zhang S.; Feng T.T.; Xu Z.Q.; Gao J.; Wu M.Q. Fastly PECVD-grown vertical carbon nanosheets for a composite SiOx-C anode material. *Appl. Surf. Sci.* **2022,** 605, 154627.
139. Zhou H.; Zhou H.P.; Yang B.; Liu C.; Zhang S.; Feng T.T.; Xu Z.Q.; Fang Z.X.; Wu M.Q. Carbon nano-onions/tubes catalyzed by Ni nanoparticles on SiOx for superior lithium storage. *Appl. Surf. Sci.* **2023**, 640, 158355.

 doi:10.20944/preprints202508.0567.v1

140. Zhou H.; Yang B.; Zhou H.; Liu C.; Zhang S.; Feng T.; Xu Z.; Fang Z.; Gao J.; Wu M. Carbon shells and carbon nanotubes jointly modified SiOx anodes for superior lithium storage. *ACS Appl. Energy Mater.* **2024**, 7, 10307-10316.
141. Meng Q.; Li G.; Yue J.; Xu Q.; Yin Y.-X.; Guo Y.-G. High-performance lithiated SiOx anode obtained by a controllable and efficient prelithiation strategy. *ACS Appl. Mater. Interf.* **2019**, 11, 32062-32068.
142. Zhang X.; Qu H.; Ji W.; Zheng D.; Ding T.; Qiu D; Qu D. An electrode-level prelithiation of SiO anodes with organolithium compounds for lithium-ion batteries. *J. Power Sources* **2020**, 478, 229067.
143. Chen S.; Wang Z.; Wang L.; Song Z.; Yang K.; Zhao W.; Liu L.; Fang J.; Qian G.; Pan F.; Yang L. Constructing a robust solid-electrolyte interphase layer via chemical prelithiation for high-performance SiOx anode. *Adv. Energ. Sust. Res.* **2022**, 3, 2200083.
144. Li Y.; Qian Y.; Zhao Y.; Lin N.; Qian Y. Revealing the interface-rectifying functions of a Li-cyanonaphthalene prelithiation system for SiO electrode. *Sci Bull* **2022**, 67, 636-645.
145. Li X.; Bian C.; Zhang J.; Hong J.; Fu R.; Zhou X.; Liu Z.; Shao G. Chemical pre-lithiation of SiOx anodes with a weakly solvating solution of polycyclic aromatic hydrocarbons for Lithium-ion batteries. *ACS Appl. Energy Mater*. **2023**, 6, 8919-8928.
146. Ji S.; Song R.; Yuan H.; Lv D.; Yang L.; Luan J.; Wan D.; Liu J.; Zhong C. Improving the initial coulombic efficiency of SiO anode materials for lithium ion batteries by carbon coating and prelithiation. *J. Electroanal. Chem.* **2024**, 959, 118141.
147. Tang Z.; Zhou Y.; Luo B.; Li D.; Zhang B. Microstructure and electrochemical performance of Li(2)CO(3)-modified submicron SiO as an anode for Lithium-ion batteries. *ACS Appl Mater Interf.* **2025**, 17, 19573-19586.
148. Song R.; Di J.; Lv D.; Yang L.; Juan J.; Yuan H.; Liu J.; Hu W.; Zhong C. Improving the electrochemical properties of SiO(x) anode for high-performance Lithium-ion batteries by magnesiothermic reduction and prelithiation. *ACS Appl Mater Interf.* **2025**, 17, 7849-7859.
149. Chung D.J.; Youn D.; Kim S.; Ma D.; Lee J.; Jeong W.J.; Park E.; Kim J.-S.; Moon C.; Lee J.Y.; Sun H.; Kim H. Dehydrogenation-driven Li metal-free prelithiation for high initial efficiency SiO-based lithium storage materials. *Nano Energy* **2021**, 89, 106378.
150. Lau V.; Kuo C.; Lan C. Objective review on commercially viable prelithiation techniques for Lithium-ion batteries. *ChemElectroChem* **2024**, 11, e202300501.
151. Jeong W.J.; Chung D.J.; Youn D.; Kim N.G.; Kim H. Double-buffer-phase embedded Si/$TiSi_2$/Li_2SiO_3 nanocomposite lithium storage materials by phase-selective reaction of SiO with metal hydrides. *Energy Storage Mater.* **2022**, 50, 740-750.
152. Chung D.J.; Youn D.; Kim J.Y.; Jeong W.J.; Kim S.; Ma D.; Lee T.R.; Kim S.T.; Kim H. Topology optimized prelithiated SiO anode materials for Lithium-ion batteries. *Small* **2022**, 18, 2202209.
153. Zhan R.; Wang X.; Chen Z.; Seh Z.W.; Wang L.; Sun Y. Promises and challenges of the practical implementation of prelithiation in Lithium-ion batteries. *Adv. Energy Mater.* **2021**, 11, 2101565.
154. Zhang Z.; Wang H.; Cheng M.; He Y.; Han X.; Luo L.; Su P.; Huang W.; Wang J.; Li C.; Zhu Z.; Zhang Q.; Chen S. Confining invasion directions of Li+ to achieve efficient Si anode material for lithium-ion batteries. *Energy Storage Mater.* **2021**, 42; 231-239.
155. Yi S.; Yan Z.; Xiao Y.; Ye C.; Qiu H.; Zhang J.; Ning P.; Yang D.; Du N. Synergistic prelithiation and in situ nitrogen doping via Li(3)N in SiO anodes: A dual-benefit pathway to achieving enhanced Li(+) kinetics and high initial coulombic efficiency. *Small* **2025**, 21, e2501524.
156. Li J.; Zhang S.; Zeng G.; Xi Z.; Khan M.D.; Biendicho J.J.; Cabot A.; Ci L.; Sun Q.; LiF-induced formation of quartz nanodomains in micron-sized SiOx anodes for durable Lithium-ion batteries. *ACS Appl. Energy Mater*. **2025**, 8, 7753-7761.
157. Li J.; Zeng G.; Horta S.; Martinez-Alanis P.R.; Jacas Biendicho J.; Ibanez M.; Xu B.; Ci L.; Cabot A.; Sun Q. Crystallographic engineering in micron-sized SiO(x) anode material toward stable high-energy-density Lithium-ion batteries. *ACS Nano* **2025**, 19, 16096-16109.
158. Wang D.; Zhou C.; Cao B.; Xu Y.; Zhang D.; Li A.; Zhou J.; Ma Z.; Chen X.; Song H. One-step synthesis of spherical Si/C composites with onion-like buffer structure as high-performance anodes for lithium-ion batteries. *Energy Storage Mater.* **2020**, 24, 312-318.

 doi:10.20944/preprints202508.0567.v1

159. Dong X.; Woo C.; Oh S.; Kim Y.; Zhang X.; Kim K.I.; Choi K.H.; Kang J.; Jeon J.; Bang H.-S.; Oh H.-S.; Yu H.K.; Mun J.; Choi J.-Y. Effect of carbonization temperature on the electrochemical performance of monodisperse Carbon/SiO_2 nanocomposites as lithium-ion batteries anode. *J. Power Sources* **2025**, 631, 236291.
160. Yang T.; Wang Y.; Yang L.; Zhang H.; Zhang M.; Ang E.H.; Zhu J. Dynamic engineering of lithiation reactions in silicon oxide with interface regulation for enhanced safety in lithium-ion batteries. *Chem. Eng. J.* **2025**, 509, 161100.
161. S. Yoo, J. Kim, B. Kang, Characterizing local structure of SiOx using confocal μ-Raman spectroscopy and its effects on electrochemical property, *Electrochimica Acta*, **2016**, 12, 68-75.
162. Xie H.; Hou C.; Yue Z.; Zhai L.; Sun H.; Lu H.; Wu J.; Yang S.; Ma Y. Facile synthesis of C, N, P co-doped SiO as anode material for lithium-ion batteries with excellent rate performance. *J. Energy Storage* **2023**, 64, 107147.
163. Suh S. S.; Yoon W.Y.; Kim D.H.; Kwon S.U.; Kim J.H.; Kim Y.U.; Jeong C.U.;Chan Y.Y.; Kang S.H.; Lee J.K.; Electrochemical behavior of SiOx anodes with variation of oxygen ratio for Li-ion batteries, *Electrochim. Acta* **2014**, 148, 111-117.
164. Raza A.; Jung J.Y.; Lee C.-H.; Kim B.G.; Choi J.-H.; Park M.-S.; Lee S.-M. Swelling-controlled double-layered SiOx/Mg_2SiO_4/SiOx composite with enhanced initial coulombic efficiency for Lithium-ion battery. *ACS Appl. Mater. Interf.* **2021**, 13, 7161-7170.
165. Cheng Y.; Wei K.; Yu Z.; Fan D.; Yan D.L.; Pan Z.; Tian B. Ternary Si-SiO-Al composite films as high-performance anodes for Lithium-ion batteries. *ACS Appl. Mater. Interf.* **2021**, 13, 34447-34456.
166. Zhang P.; Wang L.; Xie J.; Su L.; Ma C. Micro/nano-complex-structure SiOx-PANI-Ag composites with homogeneously-embedded Si nanocrystals and nanopores as high-performance anodes for lithium ion batteries. *J. Mater. Chem. A* **2014**, 2, 3776-3782.
167. Yu Z.; Yu K.; Wei J.; Lu Q.; Cheng Y.; Pan Z. Improving electrode properties by sputtering Ge on SiO anode surface. *Ceram. Int.* **2022**, 48, 26784-26790.
168. Röck A.; Wohlfahrt-Mehrens M.; Axmann P.; Hoffmann A. Improving Gr/SiO negative electrode formulations: Effect of active material, binders, and single-walled carbon nanotubes. *Batteries Supercaps* **2025**, 0, e202400764.
169. Ling Y.; Chen T.; Chen S.; Wang B.; Zeng P.; Shen S.; Yuan C.; Zhou Z.; Wang J.; Zhang L. Incorporating Co Nanoparticles into SiOx Anodes for HighPerformance Lithium-Ion Batteries. *ACS Appl. Energy Mater.* **2025**, 8, 6723-6732.
170. Gao M.; Wang D.; Zhang X.; Pan H.; Liu Y.; Liang C.; Shang C.; Guo Z. A hybrid Si@FeSiy/SiOx anode structure for high performance lithium-ion batteries via ammonia-assisted one-pot synthesis. *J. Mater. Chem. A* **2015**, 3, 10767-10776.
171. Bian C.; Fu R.; Shi Z.; Ji J.; Zhang J.; Chen W.; Zhou X.; Shi S.; Liu Z. Mg_2SiO_4/Si-coated disproportionated SiO composite anodes with high initial coulombic efficiency for lithium ion batteries. *ACS Appl. Mater. Interf.* **2022**, 14, 15337-15345.
172. Kim K.; Choi H.; Kim J.-H. Effect of carbon coating on nano-Si embedded SiOx-Al_2O_3 composites as lithium storage materials. *Appl. Surf. Sci.* **2017**, 416, 527-535.
173. Youn D.; Kim J.Y.; Lee T.R.; Han J.; Kim S.; Kim H. Al_2O_3-sheathed Si/Li_2SiO_3 nanocomposite anode materials for high-performance lithium-ion batteries. *Chem. Eng. J.* **2025**, 506, 160366.
174. Zhou M.; Gordin M.L.; Chen S.; Xu T.; Song J.; Lv D.; Wang D. Enhanced performance of SiO/Fe_2O_3 composite as an anode for rechargeable Li-ion batteries. *Electrochem. Commun.* **2013**, 28, 79-82.
175. Liao C.; Wu S. Pseudocapacitance behavior on Fe_3O_4-pillared SiOx microsphere wrapped by graphene as high performance anodes for lithium-ion batteries. *Chem. Eng. J.* **2019**, 355, 805-814.
176. Park Y.; Lee J. Silicon monoxide with black titania and carbon coating layer as an anode material for lithium-ion batteries. *Appl.Surf. Sci.* **2021**, 554, 149512.
177. Xiao Z.; Yu C.; Lin X.; Chen X.; Zhang C.; Jiang H.; Zhang R.; Wei F. TiO_2 as a multifunction coating layer to enhance the electrochemical performance of SiOx@TiO_2@C composite as anode material. *Nano Energy* **2020**, 77, 105082.

 doi:10.20944/preprints202508.0567.v1

178. Xu Y.; Li Y.; Qian Y.; Sun S.; Lin N.; Qian Y. Deficient TiO_{2-x} coated porous SiO anodes for high-rate lithium-ion batteries. *Inorg. Chem. Front.* **2023**, 10, 1176-1186.
179. Lai G.; Wei X.; Zhou B.; Huang X.; Tang W.; Wu S.; Lin Z. Engineering high-performance SiOx anode materials with a titanium oxynitride coating for Lithium-ion batteries. *ACS Appl. Mater. Interf.* **2022**, 14, 49830-49838.
180. Liu H.; Zhang X.; Xu Q. Jin Y.; Lv S.; Liu H. Oxygen vacancy-driven embedded electric fields in TiO_{2-x}/SiOx anodes for superior Lithium-ion battery performance. *ACS Sustain. Chem. Eng.* **2025**, 13, 7430–7439.
181. Zhang Y.; Guo G.; Chen C.; Jiao Y.; Li T.; Chen X.; Yang Y.; Yang D.; Dong A. An affordable manufacturing method to boost the initial Coulombic efficiency of disproportionated SiO lithium-ion battery anodes. *J. Power Sources* **2019**, 426, 116-123.
182. Long Z.; Fu R.; Ji J.; Feng Z.; Liu Z. Unveiling the effect of surface and bulk structure on electrochemical properties of disproportionated SiOx anodes. *ChemNanoMat* **2020**, 6, 1127-1135.
183. Guo P.; Wang C. Good lithium storage performance of Fe_2SiO_4 as an anode material for secondary lithium ion batteries. *RSC Adv.* **2017**, 7, 4437-4443.
184. Tang C.; Liu Y.; Xu C.; Zhu J.; Wei X.; Zhou L.; He L.; Yang W.; Mai L. Ultrafine nickel-nanoparticle-enabled SiO_2 hierarchical hollow spheres for high-performance lithium storage. *Adv. Funct. Mater.* **2018**, 28, 1704561.
185. Fu R.; Wu Y.; Fan C.; Long Z.; Shao G.; Liu Z. Reactivating Li_2O with nano-Sn to achieve ultrahigh initial coulombic efficiency SiO anodes for Li-ion batteries. *ChemSusChem* **2019**, 12, 3377-3382.
186. Zhang H.; Hu R.; Liu Y.; Cheng X.; Liu J.; Lu Z.; Zeng M.; Yang L.; Liu J.; Zhu M. Highly reversible conversion reaction in Sn2Fe@SiOx nanocomposite: A high initial Coulombic efficiency and long lifetime anode for lithium storage. *Energy Storage Mater.* **2018**, 13, 257-266.
187. Zhou Z.; Li Z.; Liu X.; Wu J.; Li K.; Wang C. Enhanced performance of yolk-shell SiO/MWCNTs@C composites bridged by MWCNTs for high-performance lithium-ion battery anodes. *Chem. Engin. J.* **2025**, 511, 162297.